JCB Journal of Cell Biology

ARTICLE

Ist2 recruits the lipid transporters Osh6/7 to ER–PM contacts to maintain phospholipid metabolism

Andrew King On Wong, Barry Paul Young, and Christopher J.R. Loewen

ER-plasma membrane (PM) contacts are proposed to be held together by distinct families of tethering proteins, which in yeast include the VAP homologues Scs2/22, the extended-synaptotagmin homologues Tcb1/2/3, and the TMEM16 homologue Ist2. It is unclear whether these tethers act redundantly or whether individual tethers have specific functions at contacts. Here, we show that Ist2 directly recruits the phosphatidylserine (PS) transport proteins and ORP family members Osh6 and Osh7 to ER–PM contacts through a binding site located in Ist2's disordered C-terminal tethering region. This interaction is required for phosphatidylethanolamine (PE) production by the PS decarboxylase Psd2, whereby PS transported from the ER to the PM by Osh6/7 is endocytosed to the site of Psd2 in endosomes/Golgi/vacuoles. This role for Ist2 and Osh6/7 in nonvesicular PS transport is specific, as other tethers/transport proteins do not compensate. Thus, we identify a molecular link between the ORP and TMEM16 families and a role for endocytosis of PS in PE synthesis.

Introduction

Lipid metabolic pathways often have steps that occur at different organelles throughout the cell (Henry et al., 2012), and thus, lipid substrates must be transported between organelles. Much of this transport occurs in a nonvesicular fashion at membrane contact sites (MCSs), where the membranes of different organelles are closely apposed, usually to within 10–30 nm (Gatta and Levine, 2017). Contacts have been observed between most organelle pairs in the cell and are likely sites of material transfer and signaling between organelles, and thus there is great interest in elucidating the functions of MCSs and their molecular constituents (Gatta and Levine, 2017).

The ER makes contact with nearly all organelles as well as the plasma membrane (PM; Wu et al., 2018). The ER makes a large number of contacts with the PM (Saheki and De Camilli, 2017), with up to 20–40% of the internal PM surface contacting the ER in yeast (West et al., 2011). ER–PM contacts, also known as PM-associated ER (pmaER; West et al., 2011), are enriched in lipid-synthesizing enzymes (Pichler et al., 2001) and are believed to be sites where lipids are transported between the ER and the PM (Maeda et al., 2013; Gatta et al., 2015), as well as sites where ER resident enzymes act in trans across the cytoplasmic gap on lipid substrates in the PM (Tavassoli et al., 2013; Stefan et al., 2011). Contacts can be formed dynamically in response to signaling events or substrate loads (Lees et al., 2017; Sandhu et al., 2018).

Lipid transport at ER–PM contacts is performed by lipid transfer proteins (LTPs). A major family of LTPs are the oxysterol-binding protein related proteins (ORPs). ORPs are conserved throughout eukaryotes, with 12 homologues in humans and 7 in yeast (Pietrangelo and Ridgway, 2018). Although ORPs may share redundant functions (Beh et al., 2001), individual ORPs seem to be involved in the transport of specific lipids. Yeast ORPs Osh6 and Osh7 and mammalian ORPs ORP5 and ORP8 have been found to bind the lipid phosphatidylserine (PS) and transport it from its site of synthesis at the ER to the PM (Maeda et al., 2013; Chung et al., 2015; Moser von Filseck et al., 2015), where it is enriched (van Meer et al., 2008). As ER-to-PM PS transport goes up a concentration gradient, PS movement is driven by countertransport of phosphatidylinositol-4-phosphate (PI4P) by Osh6/7 or ORP5/8 down its concentration gradient from the PM to the ER, where it is hydrolyzed by the PI4P phosphatase Sac1 into phosphatidylinositol (PI; Chung et al., 2015; Moser von Filseck et al., 2015).

PS is both a major lipid component of the inner leaflet of the PM and a substrate for synthesis of the other major lipids phosphatidylethanolamine (PE) and phosphatidylcholine (PC; Henry et al., 2012). In yeast, the PS decarboxylases Psd1 and Psd2 convert PS to PE, which is then converted to PC by the methyltransferases Cho2 and Opi3. Psd1 resides on the inner membrane of mitochondria (Wagner et al., 2018) and on the ER (Friedman et al., 2018), whereas Psd2 localization is less well defined and is proposed to be at endosomes (Gulshan et al., 2010), ER-endosome contact sites (Riekhof et al., 2014), and

Department of Cellular and Physiological Sciences, Life Sciences Institute, University of British Columbia, Vancouver, British Columbia, Canada.

Correspondence to Christopher J.R. Loewen: cloewen@mail.ubc.ca.

© 2021 Wong et al. This article is distributed under the terms of an Attribution–Noncommercial–Share Alike–No Mirror Sites license for the first six months after the publication date (see http://www.rupress.org/terms/). After six months it is available under a Creative Commons License (Attribution–Noncommercial–Share Alike 4.0 International license, as described at https://creativecommons.org/licenses/by-nc-sa/4.0/).

the Golgi and/or vacuoles (Trotter and Voelker, 1995). PS synthesized by the ER-localized PS synthase Cho1 is directly accessible to ER-localized Psd1 (Friedman et al., 2018) or can be delivered to mitochondrial-localized Psd1 by LTPs (Lang et al., 2015) for conversion to PE. However, it is less clear how PS is delivered to Psd2. Presumably, secretory traffic could deliver PS from the ER to the Golgi (Fairn et al., 2011) where it could be used by Golgi-localized Psd2 or trafficked to the late endosomes/vacuoles, depending on where Psd2 resides. It is not known whether Osh6/7-mediated PS transport to the PM contributes to PE synthesis, although this pool of PS would conceivably need to be delivered to the site of Psd1 or Psd2, either by endocytosis or by using an MCS.

The cytoplasmic gaps at MCSs are bridged by protein tethers that are either anchored in or bind to both membranes at a contact. Tethers presumably create MCSs by physically holding two membranes together. However, a strict definition of an MCS tether is contentious (Eisenberg-Bord et al., 2016), as nominal tethers often have functional modules such as lipid-binding domains in the linker between the two membrane anchors (Gatta and Levine, 2017). In yeast, several proteins have been reported to function as tethers at ER–PM contacts. The vesicle-associated membrane-protein-associated protein homologues Scs2/22, the extended synaptotagmin homologues Tcb1/2/3, the TMEM16 homologue Ist2 (Manford et al., 2012), and the integral membrane protein Ice2 (Tavassoli et al., 2013; Loewen et al., 2007) all presumably function redundantly as ER–PM tethers, as deletion of all seven proteins results in ER–PM contacts at levels consistent with incidental contact of the ER with the PM (Quon et al., 2018). However, these tethers are structurally diverse, suggesting specialized physiological functions. For example, *Δscs2Δice2* mutants alone are sufficient to reduce in trans activity of ER-localized Opi3 on the PM, conferring cells with a choline (Cho) auxotrophy (Tavassoli et al., 2013). Furthermore, the mammalian extended-synaptotagmins are directly capable of lipid transport via their SMP domains and are involved in the clearance of diacylglycerol from the PM (Saheki et al., 2016). Thus, distinguishing the roles of individual ER–PM tethers is important in understanding the biology of ER–PM contact sites.

Here we show that Osh6 and Osh7 directly bind to the tethering protein Ist2 to transport PS from the ER to the PM. Ist2 recruits Osh6/7 to the pmaER through a binding site in the disordered linker region of Ist2 that bridges the ER–PM gap. Loss of Osh6 and Osh7 (or ablation of their binding site in Ist2) in the absence of Psd1 results in dramatically inhibited cell growth and reduced PE synthesis, with PS delivery to Psd2 at the Golgi/endosome/vacuole requiring endocytosis.

Results

Osh6 and Osh7 physically interact with Ist2 at pmaER

Both Osh6 and its paralogue Osh7 are soluble members of the ORP family and contain only the core OSBP-related domain with no known membrane-binding domains or motifs (Raychaudhuri and Prinz, 2010). Although Osh6/7 can bind two membranes simultaneously in vitro (Schulz et al., 2009), we reasoned that Osh6/7 may need a membrane-bound partner to localize them to pmaER. We searched through high-throughput protein–protein interaction datasets and found an interaction between Osh6 and Ist2 by coimmunoprecipitation (Babu et al., 2012). Ist2 would be an ideal candidate binding partner, as it is N-terminally embedded in the ER through its multipass transmembrane TMEM16 domain and contains a C-terminal amphipathic helix that binds the PM (Fig. 1 A; Fischer et al., 2009). These modules are connected by a disordered linker that spans the intermembrane gap (Kralt et al., 2015).

To confirm the interaction of Ist2 and Osh6, we used a protein complementation assay (PCA) whereby we fused Ist2 and Osh6/7 with either the N-terminal ([1,2]) or the C-terminal ([3]) fragments of a murine dihydrofolate reductase (DHFR) mutant resistant to the drug methotrexate (Michnick et al., 2010). Protein interaction reversibly reconstitutes DHFR, allowing cells to grow in the presence of methotrexate. We found that Ist2 PCA pairs with Osh6 and Osh7 allowed growth on methotrexate, suggesting these proteins interacted in vivo (Fig. 1 B). To determine the localization of the Ist2–Osh6 and Ist2–Osh7 interaction, we used another PCA with fragments of the fluorophore Venus, allowing visualization of the intact fluorophore upon protein interaction (Michnick et al., 2010). We found that all Ist2, Osh6, and Osh7 PCA pairs resulted in a punctate fluorescence pattern at the cell periphery characteristic of pmaER (Fig. 1 C), similar to the localization of GFP-tagged Ist2, Osh6, and Osh7 (Fig. S1 A; Schulz et al., 2009; Manford et al., 2012). These data suggested that Ist2 could interact with Osh6/7 in vivo at pmaER.

Although protein complementation can be used to infer protein interaction in vivo, positive complementation signals can arise from coincidental proximity of two target proteins without direct binding. To demonstrate that this interaction is specific, we sought to locate the binding site for Osh6/7 on Ist2. We first deleted the C-terminal PM-binding region of Ist2 but found that the construct still interacted with Osh6 by Venus PCA (Fig. S1 C). However, Ist2 constructs missing both the C-terminal helix and most of the disordered linker displayed an attenuated Venus PCA signal at the cell periphery with Osh6/7, suggesting that the binding site may be located in the linker (Fig. S1 D). We aligned the linker region with fungal homologues and found that the sequence between residues 721 and 790 contained a number of conserved residues, with a core sequence between residues 732 and 747 being the most conserved (Fig. S1 E). Additionally, residues 739–747 were not predicted to be disordered (Fig. S1 F). Thus, we selected this sequence for further investigation as a binding site for Osh6/7.

Using bacteria, we expressed and purified various GST-tagged Ist2 linker peptides from the region discussed above, and then immobilized these fusion proteins onto glutathione resin. We also expressed and purified soluble MBP-tagged Osh6 and found that the Ist2 peptides were able to pull down MBP-Osh6 (Fig. 1 D). Of these peptides, residues 732–747 were sufficient to interact with Osh6, whereas further truncation into this region disrupted binding (Fig. 1 D). Thus, Ist2 bound to Osh6 directly in vitro through a binding site centered around residues 732–747.

Next, we tested if this region of Ist2 is important for binding in vivo. First, we imaged Ist2Δ732–747-GFP and found it to be

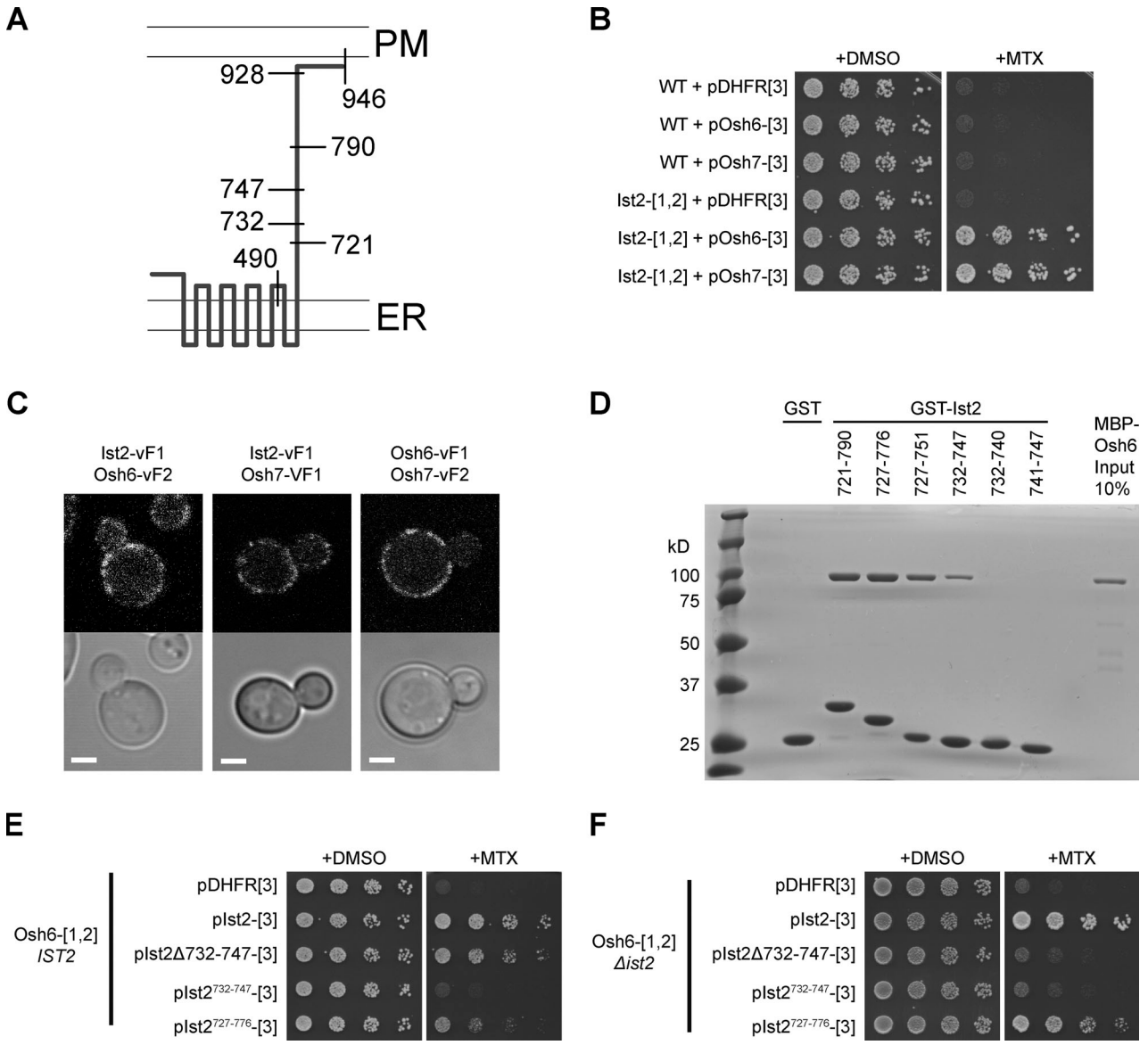

Figure 1. **Ist2 physically interacts with Osh6 and Osh7. (A)** Topology of Ist2 and key residue locations. 490: Truncation before this residue removes most of the TMEM16 domain leaving two transmembrane helices as an ER anchor. 721–790: Maximum Ist2 linker sequence explored as a binding site for LTPs Osh6/7. 732–747: Core sequence for Osh6/7 binding. 928–946: PM-binding amphipathic helix. **(B)** DHFR PCA with yeast expressing C-terminal fusion proteins. DHFR [1,2] fusions are genomically integrated; DHFR[3] fusions are plasmid expressed. WT cells contained untagged Ist2. DMSO control plates incubated for 48 h, methotrexate (MTX) plates incubated for 96 h. **(C)** Live imaging of log-phase yeast cells. Venus PCA using genomically integrated C-terminal protein fusions with fragments vF1 and vF2. **(D)** Purified recombinant GST-fusion proteins were immobilized on glutathione beads and incubated with purified recombinant MBP-Osh6 fusion protein. Bound fractions were analyzed by SDS-PAGE and Coomassie Blue staining. **(E)** As in B, except MTX plates were incubated for 72 h. **(F)** As in B. Scale bars: 2 µm.

present in cortical puncta, indicating that deleting the Osh6/7 binding site did not interfere with Ist2 localization to pmaER (Fig. S1 G). Then, we used DHFR PCA to test if residues 732–747 were necessary for binding Osh6. Unexpectedly, genomically tagged Osh6-DHFR[1,2] interacted nearly as robustly with plasmid-expressed Ist2Δ732–747-DHFR[3] as with full-length Ist2-DHFR[3] (Fig. 1 E), suggesting that this mutant is capable of interacting with Osh6. However, Ist2 likely dimerizes (Franz et al., 2007), with structural information from several TMEM16 homologues, indicating that TMEM16 domains exist as dimers (Alvadia et al., 2019; Brunner et al., 2014; Dang et al., 2017; Falzone et al., 2019). We reasoned that Ist2Δ732–747-DHFR[3] constructs may form a heterodimer with untagged Ist2 in these strains, giving an interaction signal from proximity with Osh6-DHFR[1,2] interacting with untagged Ist2. Therefore, we created Osh6-DHFR[1,2] *Δist2* cells to assess the interaction between Osh6 and mutant Ist2 homodimers exclusively. We found that, unlike full-length Ist2-DHFR[3], Ist2Δ732–747-DHFR[3] yielded a severely weakened interaction signal, suggesting that residues 732–747 are necessary for Ist2's interaction with Osh6 (Fig. 1 F). We then tested if residues 732–747 alone were sufficient for interaction with Osh6. We found that in cells both with

and without genomic *IST2*, Ist2$^{732–747}$-DHFR[3] displayed an extremely weak interaction with Osh6-DHFR[1,2] (Fig. 1, E and F). Increasing the length of the peptide to span residues 727–776 yielded a stronger interaction signal with Osh6 (Fig. 1, E and F), possibly from increased binding due to additional conserved residues (Fig. S1 E), more conformational flexibility between the peptide and the DHFR[3] tag, or better expression/stability of the construct. However, cells containing the Ist2$^{727–776}$-DHFR[3] construct did not grow as well as cells containing full-length Ist2-DHFR[3], suggesting that Ist2$^{727–776}$ does not interact as strongly with Osh6 as full-length Ist2 (Fig. 1, E and F). Taken together, these results suggest that the linker region of Ist2 centered around residues 732–747 is sufficient for binding to Osh6.

Osh6/7 are recruited to the pmaER by Ist2

Next we determined if Ist2 was responsible for localizing Osh6/7 to the pmaER. Osh6 and Osh7 have been reported to be located to the pmaER (Schulz et al., 2009; Maeda et al., 2013; Moser von Filseck et al., 2015; Lipp et al., 2019). In WT cells, Osh7-GFP fluorescence signal was strongly localized to the pmaER (Fig. 2 A), whereas we found that Osh6-GFP predominantly localized to the cytosol, with weakly fluorescent puncta at the pmaER (Fig. 2 A). Deleting *IST2* delocalized Osh6-GFP and Osh7-GFP from the pmaER into the bulk cytosol (Fig. 2 A). We measured the ratio of fluorescence at the pmaER to that in the cytosol and found that deletion of *IST2* resulted in a 69% decrease of the pmaER/cytosol ratio for Osh7-GFP and a 25% decrease for Osh6-GFP (Fig. 2 B). To further confirm the importance of Ist2 in Osh6 localization, we increased cellular levels of Ist2 in WT cells by placing an additional copy of *IST2* on a plasmid driven either by its native promoter or by a galactose-inducible promoter (Fig. 2 C). As these cells did not contain an ER marker, we measured the cell periphery:cytosol fluorescence ratio of Osh6-GFP. *IST2* driven by its native promoter increased the cell periphery:cytosol ratio by 20%, whereas galactose-inducible *IST2* increased the ratio by 28% (Fig. 2 D).

We then tested whether full-length Ist2 or Ist2Δ732–747 constructs could relocalize Osh7 in a Δ*ist2* deletion strain. We found that deleting the putative Osh6/7 binding site on Ist2 prevented recruitment of Osh7-GFP to pmaER (Fig. 2 E), resulting in a 77% decrease in the cell periphery/cytosol ratio (Fig. 2 F). To exclude the possibility of Osh6/7 being required for Ist2 localization, we tested the effect of Δ*osh6*Δ*osh7* deletion on the localization of C-terminally tagged Ist2-GFP. In WT cells, Ist2-GFP localized predominantly to the pmaER, although there was some localization to internal ER structures (Fig. 2 G). As discussed below, this construct was functional (Fig. 6 C). We compared this localization to the localization of Ist2-GFP in Δ*osh6*Δ*osh7* cells as well as WT cells containing Ist2Δ928–946-GFP, whereby the genomically integrated GFP tag truncates the PM-binding C-terminal helix, thus delocalizing Ist2 from pmaER into general ER (Manford et al., 2012; Fig. 2 G). By quantifying the ratio of fluorescence in nuclear ER compared with pmaER, we found that Δ*osh6*Δ*osh7* did not significantly alter Ist2-GFP localization compared with WT cells, whereas Ist2Δ928–946-GFP had a 48% increase in the nuclear ER/pmaER ratio (Fig. 2 H). These data suggested that Ist2 directly interacted with Osh6/7 to recruit these LTPs to the pmaER.

IST2 and OSH6/7 function in aminophospholipid metabolism

Given that PS makes up a large component of the inner leaflet of the PM and is a precursor for PE and PC (Fig. 3 A), we expected that deleting the PS transporters Osh6/7 or Ist2 should have striking physiological consequences. However, we detected no growth defects for Δ*ist2* or Δ*osh6*Δ*osh7* deletion strains (Fig. 3, B and D). We reasoned that a redundant cellular pathway may mitigate the effects of these deletions. As negative genetic interactions between two deletion mutants are often indicative of redundant pathways (Boone et al., 2007), we searched high-throughput genetic interaction datasets and found that *IST2* is annotated to have a negative genetic interaction with *PSD1* (Costanzo et al., 2010). Although Psd1 and Psd2 are located in different subcellular compartments, the presence of either enzyme is sufficient for cellular growth, whereas deletion of both enzymes results in synthetic lethality, as the cell can no longer produce PC (Storey et al., 2001). This phenotype can be alleviated by addition of exogenous ethanolamine (Etn) or Cho, which are salvaged by the Kennedy pathways to PE and PC, respectively (Fig. 3 A).

We confirmed that Δ*ist2*Δ*psd1* cells had a negative genetic interaction that could be alleviated with Etn or Cho supplementation, whereas Δ*ist2*Δ*psd2* cells did not have a genetic interaction (Fig. 3 B). We quantified the growth defects by measuring the log-phase growth rates in liquid medium (Figs. 3C and S2, A–D). WT cells had a base 2 exponential growth constant of 0.67 h^{-1} (Fig. 3 C). We found that Δ*psd2* cells had a growth constant of 0.64 h^{-1}, similar to WT, whereas Δ*psd1* cells had a mild growth defect, with a constant of 0.48 h^{-1} (Fig. 3 C). Δ*psd2*Δ*psd1* exhibited no growth unless supplemented with Etn or Cho (Fig. S2 A). Δ*ist2*Δ*psd1* cells did not have a lethal growth phenotype but grew less than Δ*psd1* cells, with a growth constant of 0.24 h^{-1} (Fig. 3 C), which is less than expected per the multiplicative model of genetic interactions (Fig. S2 E; Dixon et al., 2009), with growth restored to the rate of Δ*psd1* by addition of Etn or Cho (Fig. S2, C and D). Δ*ist2* and Δ*ist2*Δ*psd2* had growth constants of 0.67 and 0.69 h^{-1}, respectively, similar to WT cells (Fig. 3 C). These data suggested that Ist2 had a role in the same pathway as Psd2. Interestingly, Δ*ist2*Δ*psd1* cells had increased final stationary-phase cell density in the presence of Etn and Cho compared with Δ*psd1* cells (Fig. S2 A).

If Osh6/7 and Ist2 functioned in the same pathway, then deleting *OSH6/7* should also result in a genetic interaction with *PSD1*. While *OSH6* or *OSH7* deletion alone did not result in a genetic interaction with *PSD1*, Δ*osh6*Δ*osh7*Δ*psd1* cells exhibited a growth defect that was alleviated by Etn or Cho (Fig. 3 D). We measured growth rates in liquid medium and found Δ*osh6*Δ*osh7*Δ*psd1* cells had a growth constant of 0.17 h^{-1}, slightly slower than Δ*ist2*Δ*psd1* cells, with a growth constant of 0.23 h^{-1} (Figs. 3 E and S2, F–I) less than expected by the multiplicative model (Fig. S2 J). Δ*osh6*Δ*osh7*Δ*psd2* cells did not grow differently than Δ*psd2* cells (Figs. S2 F and S3 A). We expressed from plasmids either full-length Ist2 or Ist2Δ732–747 in Δ*ist2*Δ*psd1* cells and found that Ist2 complemented the growth defect of

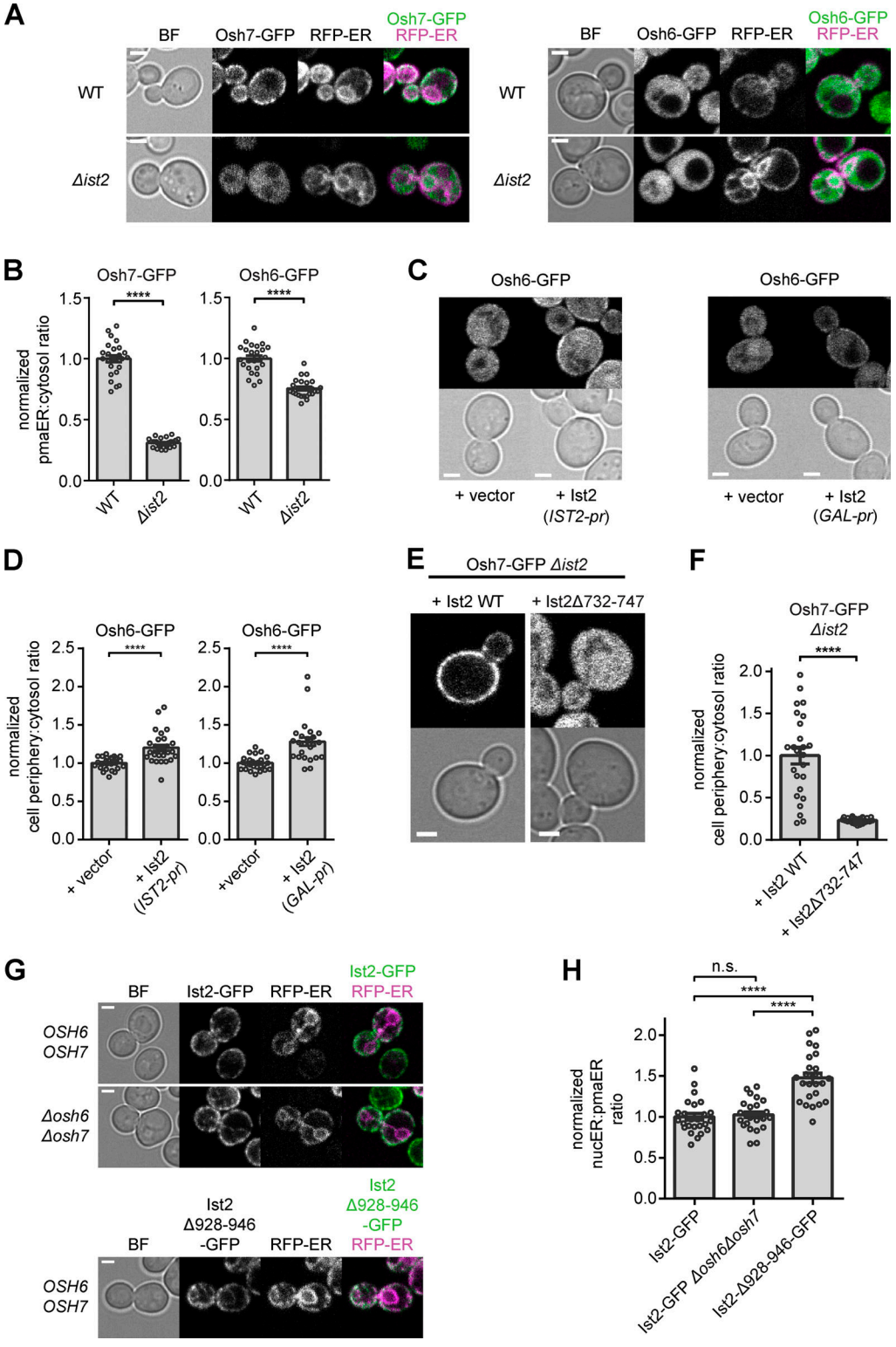

Figure 2. **Ist2 recruits Osh6 and Osh7 to ER–PM contacts. (A)** WT and *Δist2* cells expressing C-terminally tagged Osh6-/Osh7-GFP and an ER marker consisting of RFP fused to the C-terminal transmembrane helix of the ER protein Scs2 (RFP-ER). **(B)** Quantitation of A. **(C)** WT and *Δist2* cells expressing C-terminally tagged Osh6-GFP, expressing plasmid-borne Ist2 on its native promoter (*IST2-pr*) or under a *GAL* promoter (*GAL-pr*). **(D)** Quantitation of cells from C. **(E)** Localization of Osh7-GFP in *Δist2* cells expressing plasmid-borne WT Ist2 or mutant Ist2Δ732–747. **(F)** Quantitation of cells from E. **(G)** WT (*OSH6OSH7*) and *Δosh6Δosh7* cells expressing C-terminally tagged Ist2-GFP or Ist2-Δ928–946-GFP (missing its PM-binding helix) and RFP-ER. **(H)** Quantitation of G. BF, bright field; nucER, nuclear ER. Scale bars: 2 µm. Data are mean ± SEM, $n = 25$. ****, $P < 0.0001$.

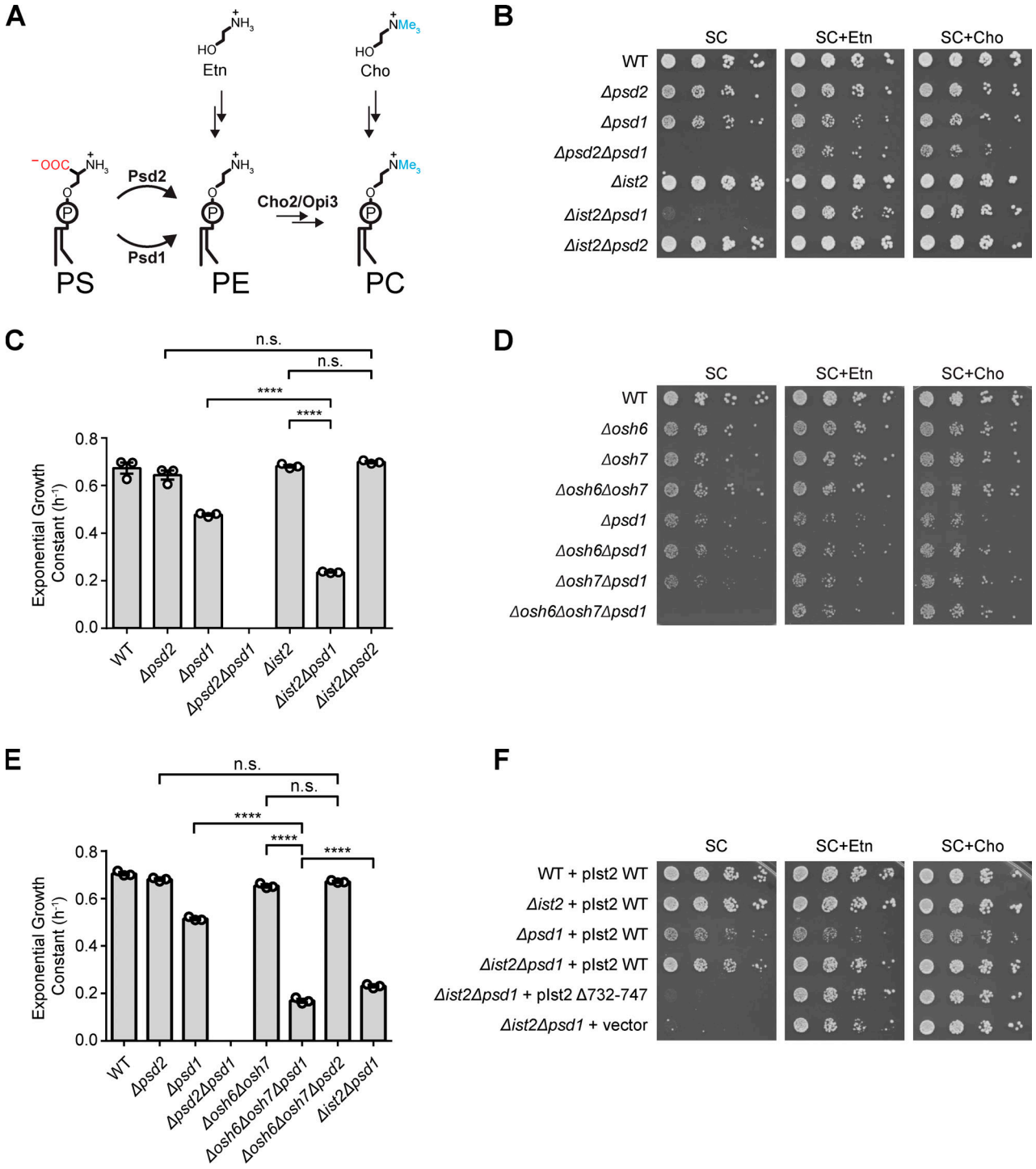

Figure 3. **Ist2, Osh6, and Osh7 function in aminophospholipid metabolism. (A)** Schematic depicting aminophospholipid metabolism. Me, methyl group. **(B)** Serial dilutions of the indicated yeast strains grown on SC agar medium with or without Etn or Cho. **(C)** Base 2 exponential growth constants calculated from liquid cultures of yeast in SC medium without Etn or Cho. **(D and E)** As in B and C. **(F)** Serial dilutions of indicated yeast strains expressing plasmid-borne WT Ist2 or mutant Ist2Δ732–747 driven by their native promoter, grown on SC agar medium with or without Etn or Cho. ****, P < 0.0001. Data are mean ± SEM, *n* = 3.

Δist2Δpsd1 cells, but Ist2Δ732–747 could not (Fig. 3 F). These results were consistent with binding between Ist2 and Osh6/7 being required for their function in the Psd2 pathway.

We sought to further characterize the position of Ist2 and Osh6/7 in the Psd2 pathway. We found that overexpression of Osh6 or Osh7 alleviated the growth defect of *Δist2Δpsd1*, whereas overexpression of Ist2 did not alleviate the *Δosh6Δosh7Δpsd1* growth defect, indicating that Osh6/7 functioned downstream of Ist2 (Fig. 4, A–C). We then overexpressed Psd2 in *Δist2Δpsd1* and *Δosh6Δosh7Δpsd1* cells and found that Psd2 alleviated their

growth defects (Fig. 3 D), whereas overexpression of Ist2 or Osh7 did not alleviate the growth defect of *Δpsd2Δpsd1* cells (Fig. S3 C), indicating Psd2 acted downstream of Ist2 and Osh6/7. Furthermore, overexpression of Cho2 or Opi3 failed to rescue *Δist2Δpsd1* and *Δosh6Δosh7Δpsd1* cells (Fig. S3, D and E), consistent with Ist2/Osh6/7 participating in a step proximal to Psd2 and PE synthesis, as rescue by Cho2/Opi3 would depend on sufficient PE production. Thus, Ist2 functioned upstream of Osh6/7, which functioned upstream of Psd2.

To test if lipid counter transport ability was indeed required for Osh6/7 function in the Psd2 pathway, we introduced the L69D binding-pocket mutation into both Osh6/7, which ablates their ability to bind PS and PI4P (Maeda et al., 2013; Moser von Filseck et al., 2015). We found that Osh6/7 L69D was unable to complement *Δosh6Δosh7Δpsd1* cells (Fig. 5 A). Additionally, the PI4P phosphatase Sac1 is believed to function on the ER membrane to hydrolyze PI4P delivered by Osh6/7 from the PM to the ER in order to maintain a PI4P gradient between the PM and the ER and create a motive force to drive countertransport of PS from the ER to the PM (Moser von Filseck et al., 2015; Zewe et al., 2018). We found that simultaneous deletion of *Δsac1* and *Δpsd1* resulted in a negative genetic interaction that was rescued by addition of Etn or Cho (Fig. 5 B), indicating that Sac1 was required for PE synthesis by Psd2. Taken together, these results strongly support that PS transport by Osh6/7 is important for their function in aminophospholipid metabolism.

Tethering by Ist2 is necessary for its role in the Psd2 pathway

Ist2 is composed of a large N-terminal multipass transmembrane domain region followed by a disordered linker region, and terminating in a C-terminal amphipathic helix that binds PM lipids (Fig. 6 A; Fischer et al., 2009). The transmembrane region, though highly conserved with the TMEM16 family of lipid scramblases and ion channels, has not been demonstrated to have lipid scramblase activity (Malvezzi et al., 2013). However, the transmembrane domain also provides an anchor into the ER membrane and is mostly dispensable for its pmaER tethering ability, provided a minimal number of transmembrane helices are left intact (Manford et al., 2012). Deleting the entirety of the transmembrane region or the PM-binding helix compromises the tethering ability of Ist2, resulting in loss of large regions of pmaER in a strain deleted of several other redundant pmaER tethering proteins (Manford et al., 2012). Thus, ER and PM membrane anchoring are essential for Ist2's tethering function.

To assess whether the tethering ability or putative scramblase/channel activity is required for Ist2 function in the Psd2 pathway, we constructed several GFP-tagged truncation mutants of Ist2 (Fig. 6 B) in the presence of a *Δpsd1* deletion (Fig. 6 C). N- or C-terminal tagging of Ist2 (GFP-Ist2 and Ist2-GFP, respectively) in the presence of *Δpsd1* did not result in low growth on medium lacking Etn, indicating tagging Ist2 at either terminus produced a functional protein (Fig. 6 C). Deletion of the C-terminal PM-binding helix of Ist2 (Ist2Δ928–946-GFP) mislocalized Ist2 from exclusively at pmaER to the general ER, including the nuclear envelope (Fig. 6 B), leading to a severe negative genetic interaction with *Δpsd1* (Fig. 6 C). Deleting the linker and the ER-embedded domain, leaving only the PM-binding domain (GFP-Ist2Δ1–927) also resulted in a severe growth defect in the presence of *Δpsd1* (Fig. 6 C). We then N-terminally truncated the majority of the ER embedded transmembrane region of Ist2 from residues 1–490, yielding a tethering-capable mutant that was lacking the putative scramblase/channel-forming region (GFP-Ist2Δ1–490) and found that this mutant did not have a negative genetic interaction with *Δpsd1* (Fig. 6 C). Furthermore, to reconstitute tethering by the C-terminal region of Ist2 without any of its transmembrane helices, we fused residues 589–946 of Ist2 to the C-terminus of the type I transmembrane protein Snd3, including GFP as a spacer, resulting in the construct Snd3-GFP-Ist2$^{589–946}$ (Fig. 6 A). We found that Snd3-GFP-Ist2$^{589–946}$ localized to cortical puncta typical of pmaER, indicating this region of Ist2 was sufficient for tethering when fused to an ER anchor (Fig. 6 D). Snd3-GFP-Ist2$^{589–946}$ complemented the growth defect of *Δist2Δpsd1* cells (Fig. 6 E), indicating that the tethering function of Ist2 was necessary and sufficient for its activity in the Psd2 pathway.

Osh6/7 and Ist2 have a specific role in the Psd2 pathway

While different Osh proteins have been shown to bind different lipid substrates, deletion of all seven members results in a lethal phenotype, suggesting that the entire family shares an essential function (Beh et al., 2001). Thus, we wondered if other Osh proteins could compensate for Osh6/7 function. Overexpression of other Osh family members did not rescue the growth defect of either *Δist2Δpsd1* or *Δosh6Δosh7Δpsd1* cells, suggesting that Osh6/7 function in the Psd2 pathway was specific to these two Osh proteins (Fig. 7, A and B).

To assess if other pmaER tethers could compensate for the loss of Ist2, we overexpressed Scs2 and the tricalbin Tcb3 in *Δist2Δpsd1* and *Δosh6Δosh7Δpsd1* cells. Although Scs2 and Tcb3 mildly alleviated the *Δist2Δpsd1* growth defect, they did not fully compensate for the loss of Ist2 (Fig. 7 C). Scs2 and Tcb3 overexpression had only a very minor alleviating effect on the *Δosh6Δosh7Δpsd1* growth defect, suggesting the effect observed with *Δist2Δpsd1* cells was indirect and mediated through Osh6/7 (Fig. 7 D). Thus, tethering and recruitment of Osh6/7 to pmaER by Ist2 played a specific physiological role in the Psd2 pathway.

Ist2 and Osh6/7 contribute to maintenance of PE levels in the absence of Psd1

The strong growth defect of *Δist2Δpsd1* and *Δosh6Δosh7Δpsd1* cells suggested that aminophospholipid metabolism may be disrupted. To assess this, we extracted lipids from log-phase cells growing without Etn/Cho supplementation and measured steady-state PE levels relative to combined PS + PE + PC + PI levels after separation by TLC. Compared with WT, *Δpsd2* and *Δpsd1* cells had PE levels of 70% and 44%, respectively (Fig. 8 A and Fig. S4). As *Δpsd2Δpsd1* double mutants are obligate Etn/Cho auxotrophs, we grew these cells with Cho and found PE levels to be 13% of WT (Fig. 8 A). Residual PE in *Δpsd2Δpsd1* is due to catabolism of sphingolipids via Dpl1 to produce phosphoethanolamine that is incorporated into PE by the Kennedy pathway (Fig. 8 C) and likely represents the base level of PE required for cell survival in the presence of Cho (Storey et al., 2001). *Δist2* and *Δosh6Δosh7* cells did not have significantly different PE levels compared

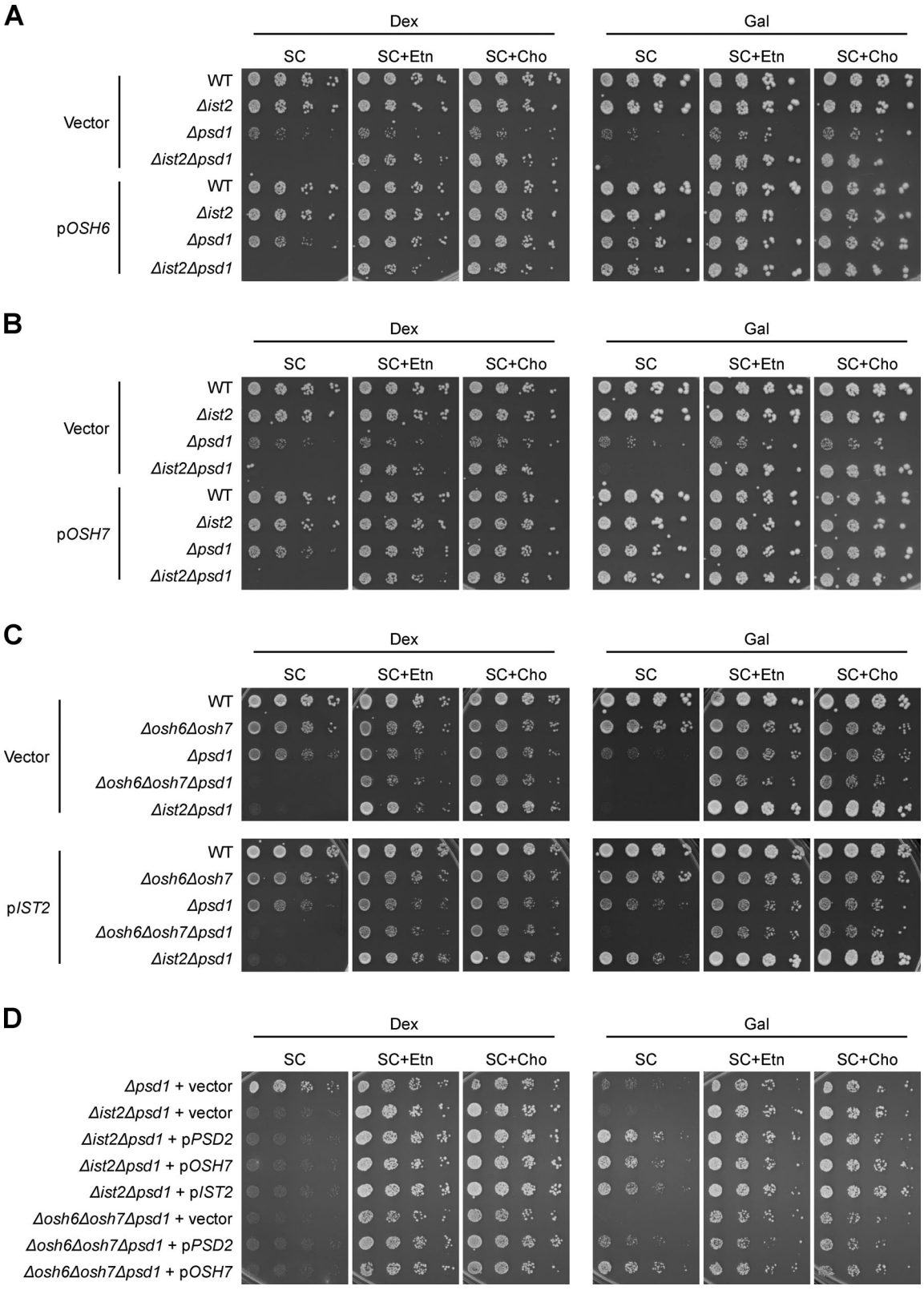

Figure 4. **Ist2 functions upstream of Osh6/7, which function upstream of Psd2. (A and B)** Serial dilutions of yeast grown on SC medium with 2% dextrose (Dex) or 2% galactose (Gal), with or without Etn or Cho, containing plasmids for overexpression of Osh6 (p*OSH6*) or Osh7 (p*OSH7*) under a galactose-inducible *GAL* promoter. Gal-containing plates were incubated for 5 d. **(C)** As in A, but with plasmids for Ist2 overexpression (p*IST2*). **(D)** As in A, but with plasmids for overexpression of Psd2 (p*PSD2*), Ist2, and Osh7. Gal-containing plates were incubated for 3 d.

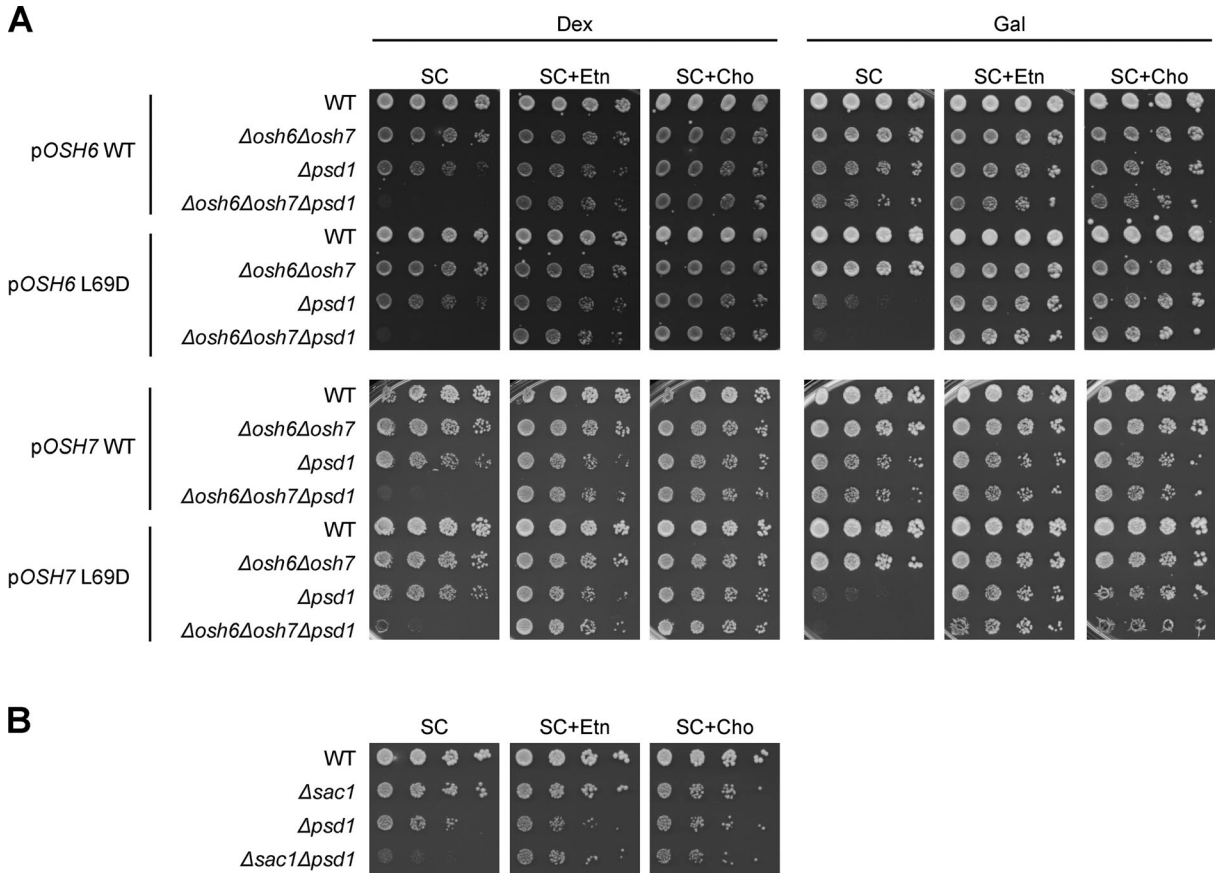

Figure 5. **Osh6/7 function is dependent on lipid-binding and the ER–PM PI4P gradient generated by Sac1. (A and B)** Serial dilutions of yeast grown on SC medium with 2% dextrose (Dex) or 2% galactose (Gal), with or without Etn or Cho supplementation, containing plasmids for overexpression of WT (p*OSH6*, p*OSH7*) or the L69D lipid-binding mutants of Osh6/7 (p*OSH6* L69D, p*OSH7* L69D) under a *GAL* promoter. Gal-containing plates were incubated for 4 d (bottom) or 5 d (top). **(B)** Serial dilutions of yeast grown on SC medium with 2% Dex, with or without Etn or Cho.

with WT (Fig. 8 A). However, *Δist2Δpsd1* and *Δosh6Δosh7Δpsd1* cells had PE levels 29% and 23% of WT, respectively, a significant decrease compared with *Δpsd1* (Fig. 8 A). These levels were not as low as *Δpsd2Δpsd1* cells grown with Cho (Fig. 8 A), consistent with *Δist2Δpsd1* and *Δosh6Δosh7Δpsd1* cells having limited residual growth without Cho, possibly because a low level of PS could still reach Psd2 via vesicular transport (Fairn et al., 2011) or other MCSs (Riekhof et al., 2014). Indeed, vesicular transport of PS or alternate LTPs/MCSs could also explain the lack of effect on PE levels by *Δist2* and *Δosh6Δosh7* deletion. Furthermore, complementation of *Δist2Δpsd1* cells with plasmid-borne WT Ist2 restored PE to *Δpsd1* levels, whereas mutant Ist2Δ732–747 did not (Fig. 8 B). Thus, transport of PS by Ist2/Osh6/7 at ER–PM contacts was required to maintain cellular PE levels in the absence of Psd1.

Deletion of *DPL1* in *Δpsd2Δpsd1* cells results in lethality even with Cho supplementation, as *Δdpl1Δpsd2Δpsd1* cells no longer have any residual PE and thus are obligate Etn auxotrophs (Fig. 8 C; Storey et al., 2001; Birner et al., 2001). We reasoned that blocking PE synthesis through sphingolipid catabolism should exacerbate the growth defect of *Δist2Δpsd1* and *Δosh6Δosh7Δpsd1* cells because of their deficiency in PE synthesis. We created *Δdpl1Δist2Δpsd1* and *Δdpl1Δosh6Δosh7Δpsd1* strains and found that these strains possessed a further growth defect compared with *Δist2Δpsd1* and *Δosh6Δosh7Δpsd1* cells unless supplemented by either Etn or Cho (Fig. 8 D). As *Δdpl1Δist2Δpsd1* and *Δdpl1Δosh6Δosh7Δpsd1* strains were not obligate Etn auxotrophs, small amounts of PS must still be able to reach Psd2 for residual PE synthesis, possibly via the secretory pathway. Additionally, we blocked upstream sphingolipid metabolism in *Δosh6Δosh7Δpsd1* cells via treatment with myriocin, a serine palmitoyl transferase inhibitor (Fig. 8 C). We found that *Δosh6Δosh7Δpsd1* cells grown without Etn or Cho were more sensitive to myriocin than WT cells (Fig. 8 E). Taken together, these results support that PS transported by Osh6/7 from ER to PM at ER–PM contacts is upstream of Psd2 in PE and PC production in aminophospholipid metabolism.

PS is delivered from the PM to Psd2 in the secretory pathway by endocytosis

To determine how Osh6/7-mediated PS transport contributed to PE synthesis by Psd2, we performed an unbiased genome-wide genetic interaction screen to identify factors required for PE synthesis by Psd2. We reasoned that this might also provide further functional evidence indicating which processes and/or subcellular compartments are required for Psd2 activity. We performed a synthetic genetic array (SGA) experiment (Tong

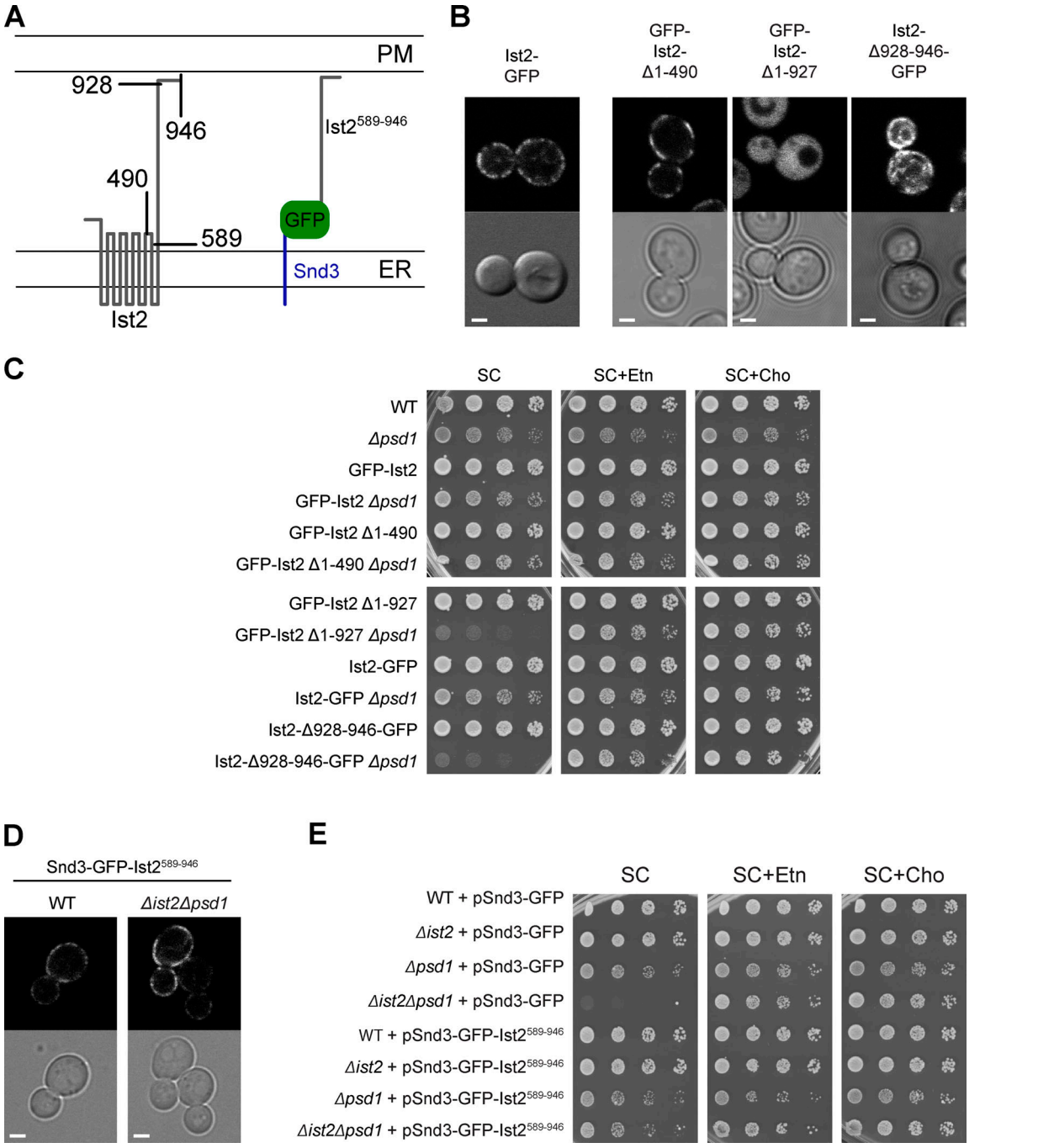

Figure 6. **Tethering by Ist2 is necessary for its role in the Psd2 pathway. (A)** Key Ist2 residues for truncation mutants, and the construct Snd3-GFP-Ist2$^{589–946}$. Truncation before residue 490 removes most of the TMEM16 domain while leaving two transmembrane helices as an ER anchor. Residues 928–946 form a PM-binding amphipathic helix. **(B)** Yeast cells expressing genomically tagged Ist2 fusion proteins. Ist2-GFP and Ist2-Δ928–946-GFP are C-terminally tagged; GFP-Ist2-Δ1–490 and GFP-Ist2-Δ1–927 are N-terminally tagged. **(C)** Serial dilutions of yeast grown on SC medium with 2% dextrose (Dex), with or without Etn or Cho. **(D)** WT or *Δist2Δpsd1* cells expressing plasmid-borne Snd3-GFP-Ist2$^{589–946}$. Medium was supplemented with Etn and Cho. **(E)** As in C. Scale bars: 2 µm.

and Boone, 2006) and obtained genetic interaction data for *PSD1* with ∼4,800 nonessential genes, in both the presence and absence of Etn. As *PSD2* is essential in the absence of *PSD1*, negative genetic interactions with *PSD1* alleviated by Etn addition will identify genes/pathways involved in *PSD2* function. Our screen identified 74 genes showing substantial negative genetic interactions with *PSD1* (i.e., at least a twofold effect) that were rescued by Etn (Fig. S4). These genes were enriched in gene ontology annotations associated with Golgi, endosomal, and vacuolar transport; retrograde transport; and vesicle organization and/or fusion (Fig. 9 A), thus supporting that Psd2 function is tied to the secretory pathway, and consistent with previous reports that it localizes to various compartments within the secretory pathway (Trotter and Voelker, 1995; Gulshan et al., 2010).

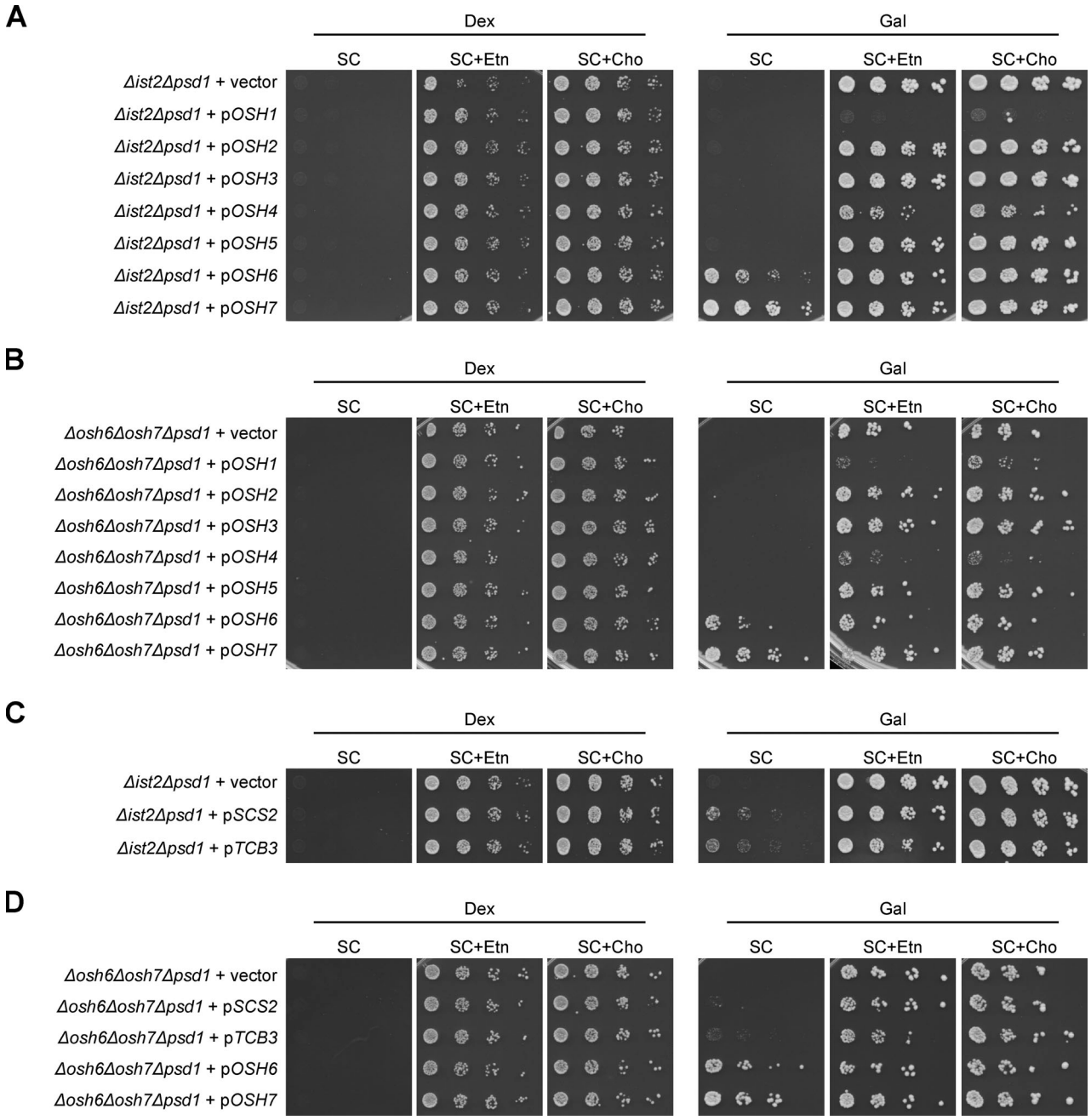

Figure 7. **Osh6/7 and Ist2 have a specific role in the Psd2 pathway.** Serial dilutions of yeast grown on SC medium with 2% dextrose (Dex) or 2% galactose (Gal), with or without Etn or Cho, containing plasmids for overexpression of the indicated proteins under a *GAL* promoter. Gal-containing plates were incubated for 5 d. **(A and B)** Overexpression of Osh family homologues (p*OSH1-OSH7*) in *Δosh6Δosh7Δpsd1* and *Δist2Δpsd1* deletion strains. **(C and D)** Overexpression of ER–PM tethers Scs2 (p*SCS2*) and Tcb3 (p*TCB3*) in *Δosh6Δosh7Δpsd1* and *Δist2Δpsd1* deletion strains.

Examining the genetic interactions more closely, we found enrichment for key complexes involved in Golgi trafficking, including the conserved oligomeric Golgi complex involved in Golgi vesicle tethering, the Golgi-associated retrograde protein complex involved in promoting fusion of transport vesicles with the TGN, various Golgi SNAREs, and Rab GTPases and Rab effectors involved in determining Golgi structure (Fig. 9 B; Miller and Ungar, 2012; Goud et al., 2018; Bonifacino and Hierro, 2011). Also present were components/complexes involved in late endosome/vacuole biogenesis, such as ESCRT-III, the ubiquitin hydrolase Doa4, the SNARE Vam7, the Rab GTPase Vps21, and the HOPS complex member Vps41 (Fig. 9 B; Balderhaar and Ungermann, 2013; Henne et al., 2011; Ungermann and Wickner, 1998). We also noted identification of a key component of the endocytic machinery, Rvs167, a Bin, Amphiphysin, RVS (BAR) domain-containing protein, which is required for scission of endocytic vesicles (Goode et al., 2015). It is likely that these components were required for localizing Psd2 to the correct compartment, trafficking PS to the Psd2 compartment, and/or biogenesis of the compartment itself.

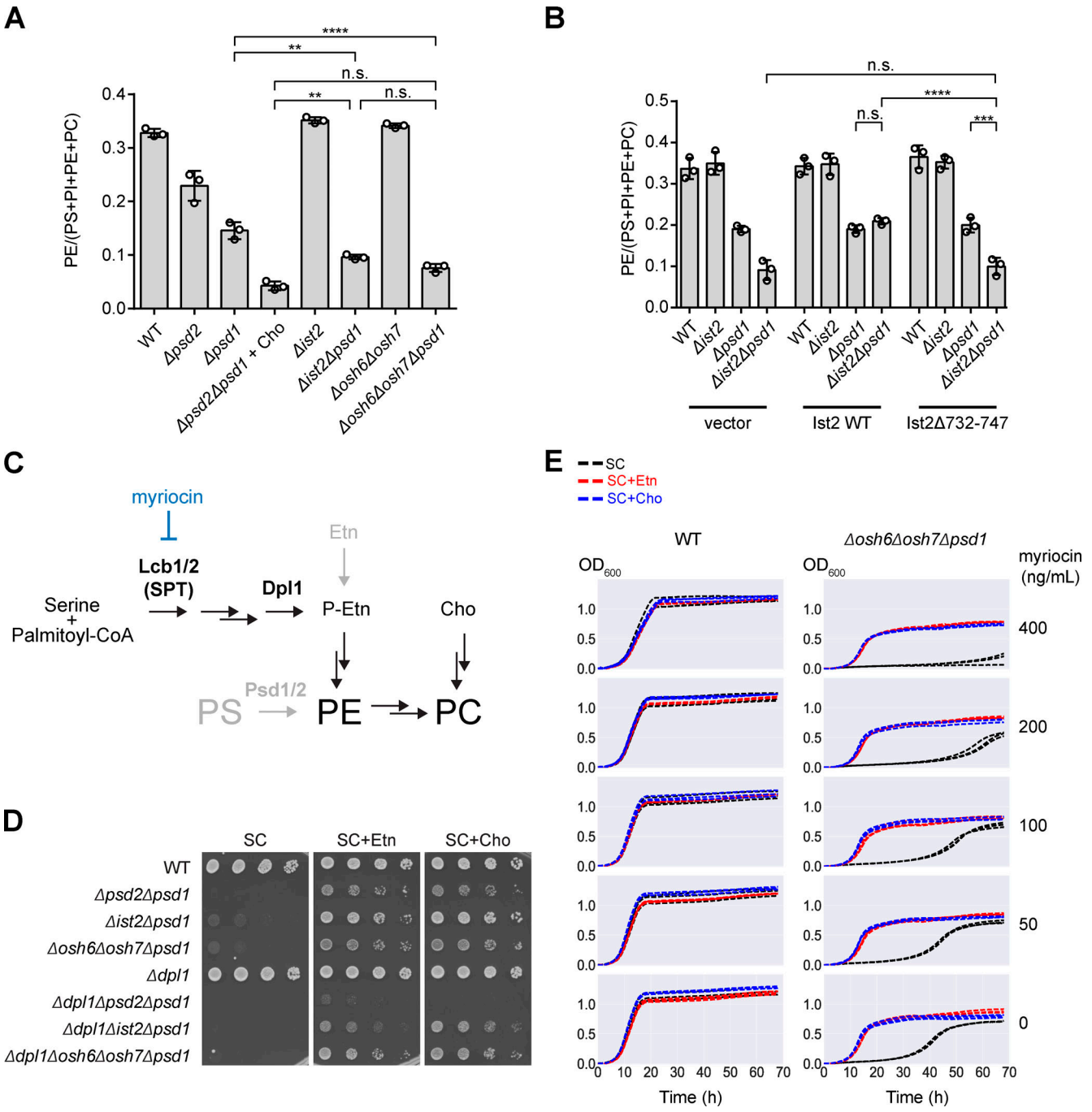

Figure 8. **Ist2 and Osh6/7 contribute to maintenance of PE levels in the absence of Psd1. (A)** PE levels relative to the total of PS, PI, PE, and PC levels. Lipids were extracted from cells during log-phase growth and separated by TLC. *Δpsd2Δpsd1* cells were grown in the presence of Cho. **(B)** As in A, but for cells expressing WT or Osh6/7-binding mutants of Ist2. **(C)** Schematic depicting the contribution of sphingolipid catabolism to PE synthesis. Myriocin inhibits serine palmitoyl transferase (SPT). P-Etn, phosphoethanolamine. **(D)** Serial dilutions of yeast grown on SC medium with 2% dextrose (Dex), with or without Etn or Cho. **(E)** Growth curves of yeast strains grown in liquid SC medium with or without Etn or Cho, with indicated concentrations of myriocin delivered in 0.4% DMSO. ****, P < 0.0001; *** P < 0.001; **, P < 0.01. Data are mean ± SEM, *n* = 3.

Nevertheless, they support that Psd2 functions in the secretory pathway.

The genetic interaction between *RVS167* and *PSD1* suggested that actin-mediated endocytosis could be the mechanism for delivery of PS from the PM to Psd2 in the secretory pathway. We verified the genetic interaction by liquid growth assay and found that the double mutant was indeed slow growing relative to either of the single mutants, and that this growth phenotype was greater than predicted by the multiplicative model, indicating a negative genetic interaction (Figs. 9 C and S5, A–E). Addition of Etn partially rescued this interaction, and addition of Cho fully rescued it (Fig. S5, A–E), supporting that the growth phenotype is linked to reduced PE synthesis. Hence, we measured PE levels in these strains. We found that the *Δrvs167* mutant had PE levels

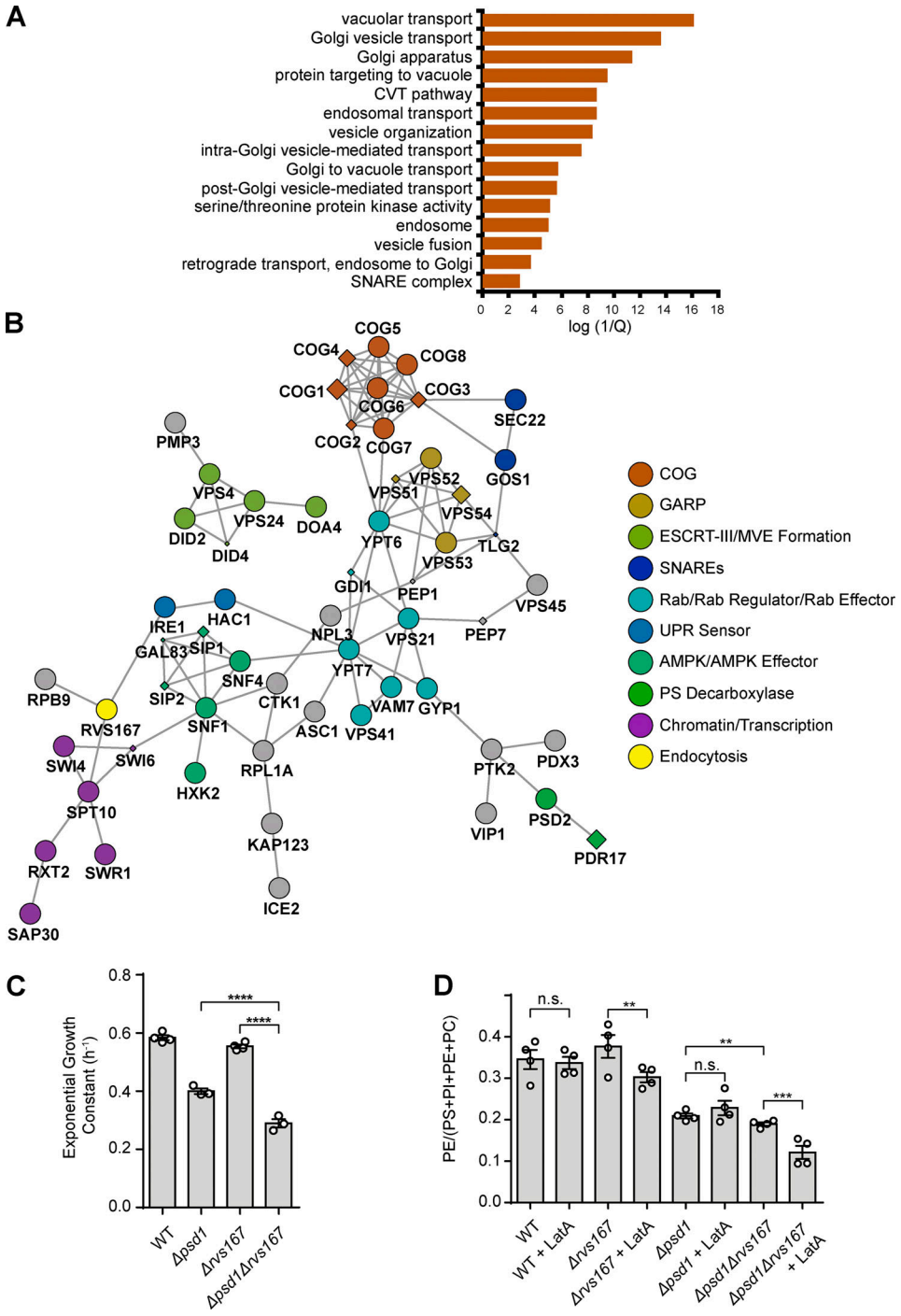

Figure 9. **PS is delivered to Psd2 at the Golgi/endosomes/vacuoles by endocytosis. (A)** Enriched gene ontology term annotations for strong *Δpsd1*-negative genetic interactors rescued by Etn. *q* Values are false discovery rate–adjusted P values from hypergeometric tests. **(B)** Protein interactions among gene sets with strong *Δpsd1*-negative genetic interactors rescued by Etn. Edges indicate annotated protein interactions found by the GeneMANIA plugin for Cytoscape. Circles indicate genes found in the SGA screen. Diamonds indicate additional genes not found in the SGA screen, but having protein–protein interactions with screen hits and predicted to be functionally related. Diamond node sizes correspond to GeneMANIA scores. AMPK, AMP-activated protein kinase; COG, conserved oligomeric Golgi; ESCRT, endosomal sorting complexes required for transport; GARP, Golgi-associated retrograde protein; MVB, multivesicular body; UPR, unfolded protein response. **(C)** Base 2 exponential growth constants calculated from liquid cultures of yeast in SC medium without Etn or Cho. **(D)** PE levels relative to the total of PS, PI, PE, and PC levels. Lipids were extracted from cells during log-phase growth and separated by TLC. ****, P < 0.0001; *** P < 0.001; **, P < 0.01. Data are mean ± SEM, *n* = 4.

similar to WT and that the *Δrvs167Δpsd1* double mutant had significantly reduced PE relative to *Δpsd1* cells, although decrease was small (Figs. 9 D and S5 G). The modest decrease in PE was perhaps not unexpected given the modest decrease in growth of the double mutant relative to *Δpsd1* cells and was likely due to inefficient disruption of endocytosis in the *Δrvs167* mutant, since it showed no growth defect and had PE levels similar to thaose of WT (Fig. 9, C and D). Therefore, we sought to disrupt endocytosis further by addition of Latrunculin A (LatA), an actin monomer-sequestering drug that inhibits endocytosis (Ayscough et al., 1997). We found a concentration of LatA (1.5 µM) that substantially inhibited growth of the *Δrvs167* mutant (to the level of the *Δrvs167Δpsd1* double mutant) without affecting WT growth (Fig. S5 F). Importantly, this chemical genetic interaction indicated we achieved specific disruption of actin mediated-endocytosis rather than generally disrupting actin-mediated processes. Next, we measured PE levels in these strains after LatA treatment. LatA did not reduce PE levels in WT but significantly reduced PE in the *Δrvs167* mutant (Figs. 9 D and S5 G), supporting a role for endocytosis in PE synthesis. LatA treatment of *Δrvs167Δpsd1* cells caused a substantial reduction in PE levels compared with untreated cells and reduced PE to nearly 50% of *Δpsd1* cells treated with LatA, indicating a substantial disruption when endocytosis was blocked. Additionally, we tested another endocytosis mutant, *Δvrp1*, which encodes yeast verprolin, a homologue of Wiskott-Aldrich syndrome protein–interacting protein (Donnelly et al., 1993; Ramesh et al., 1997), and causes defects in actin nucleation and endocytosis (Donnelly et al., 1993; Munn et al., 1995; Naqvi et al., 1998; Sun et al., 2006). We found that *Δvrp1Δpsd1* cells showed a slow growth defect relative to *Δpsd1*, indicative of a negative genetic interaction, which was rescued by Etn and Cho (Fig. S5 H). The *Δvrp1Δpsd1* phenotype was made substantially worse by addition of LatA and was rescued by Etn (Fig. S5 I). Thus, together, these data strongly supported a role for endocytosis in PE synthesis by Psd2.

Discussion

We present a model where Osh6/7 bind directly to the linker of Ist2 to localize at ER–PM contacts for the transport of PS from the ER to the PM (Fig. 10), requiring tethering by Ist2. This is important for maintaining aminophospholipid metabolism and cell growth in the absence of the ER/mitochondria-localized Psd1, without which PS from the PM must then be delivered to Psd2 via endocytosis. In the absence of both Ist2/Osh6/Osh7 and Psd1, minimal levels of delivery of PS to Psd2 likely occurs via the secretory pathway (Fairn et al., 2011), allowing residual growth of *Δist2Δpsd1* and *Δosh6Δosh7Δpsd1* cells. Thus, PS transported by Ist2 and Osh6/7 is linked to cellular lipid metabolism and does not represent a transport dead end, i.e., a terminal location for PS transport. As the two PS decarboxylases reside in separate compartments in the cell, such redundancy may become necessary when the cell encounters specific environmental challenges. Additionally, delivery of PS to the PM via Osh6/7-mediated transport also likely represents a mechanism to enrich PS in the PM before its consumption by either Psd1 or Psd2. Indeed, loss of Osh6/7 results in reduced PS as a result of increased consumption by Psd1 (Maeda et al., 2013). The role for Ist2 in recruiting Osh6/7 to ER–PM contacts for PS transport has been corroborated by another group, who additionally showed that this interaction indeed protects PS from consumption by Psd1 (D'Ambrosio et al., 2020).

While many tethers may contribute to the formation of ER–PM contacts, our data support that Ist2 is functionally specialized to transport PS from the ER to the PM. Functional specialization may be a property of many ER–PM tethers, as tethers do not necessarily overlap in localization at ER–PM contacts (Besprozvannaya et al., 2018), and many tethers are recruited in a dynamic and regulatable fashion (Lees et al., 2017). Similarly, our findings indicated that of the seven Osh homologues, only Osh6/7 functioned in aminophospholipid metabolism despite the known localization of Osh2/3 to ER–PM contacts (Schulz et al., 2009). Osh2/3, but not Osh6/7, interact with the myosin Myo5 and Scs2 for targeted delivery of sterols to endocytic sites adjacent to ER–PM contacts (Encinar Del Dedo et al., 2017), corroborating that Osh proteins are functionally specialized at ER–PM contacts.

Our work establishes a novel physical interaction between members of the TMEM16 and ORP families. The 10 human TMEM16 homologues share a core TMEM16 domain of ∼700 amino acids, with several of these homologues having additional N- and C-terminal extensions and/or loops between transmembrane sequences (Milenkovic et al., 2010; Pelz et al., 2018). It is possible these extensions contain binding sites for ORP proteins, although such sites may be hard to detect by sequence homology if they reside in disordered peptide sequences. The PS-binding mammalian homologues of Osh6/7, ORP5 and ORP8, which are anchored to the ER via transmembrane domains and bind the PM through Pleckstrin-homology domains, would presumably not require a TMEM16 binding partner to maintain localization to ER–PM contacts. However, the long splice variant of ORP8, ORP8L, localizes to general ER (Chung et al., 2015), and both ORP5 and ORP8 have a secondary localization at ER-mitochondria contacts (Galmes et al., 2016). Thus, it is conceivable that some ORP family members require targeting by TMEM16 proteins, especially considering several TMEM16 proteins are internally localized within the cell (Duran et al., 2012), raising the possibility TMEM16 proteins may function at various MCSs. Indeed, the cytosolic N-terminal region of TMEM16A has been found to bind phosphatidylinositol 4,5-bisphosphate–containing liposomes and can functionally replace the C-terminal helix of Ist2 for PM binding (Fischer et al., 2009), while TMEM16H localizes to ER–PM contacts upon ER Ca^{2+} depletion to regulate STIM1-Orai function (Jha et al., 2019). Whether TMEM16 proteins recruit ORP proteins may prove to be a fertile area of discovery for novel physiological functions that require coupling of these two protein families.

Materials and methods

Yeast strains, growth conditions, and manipulations

All yeast strains are derived from S288C. Deletion and GFP-tagged strains were constructed in the BY4741 and BY4742 backgrounds using homologous recombination of PCR-generated

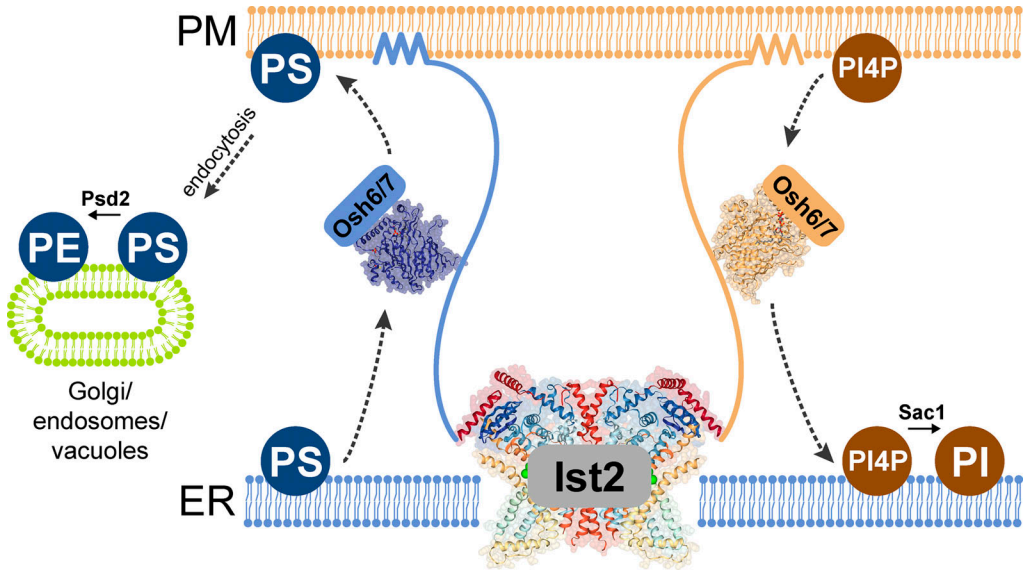

Figure 10. **Model for Ist2/Osh6/7 function in aminophospholipid metabolism.** Binding of Osh6/7 to the unstructured linker of Ist2 recruits them to ER–PM contacts, allowing PS transport from the ER to the PM, with downstream conversion to PE at the Golgi/endosomes/vacuoles after endocytosis; and concurrent PI4P countertransport from the PM to the ER, where it is hydrolyzed to PI by Sac1. Structures are illustrative only and are not drawn to scale, and a nhTMEM16 dimer is used in place of Ist2 (Protein Data Bank: accession no. 4WIS).

linear fragments amplified from pKT128, pKT209, pKT127, pRS415, pHVF1CT, pUVF2CT, or p4339 (Sheff and Thorn, 2004; Tong and Boone, 2006; Chao et al., 2014), with successful recombination assessed by colony PCR. Strains containing multiple deletions were generated either by multiple rounds of homologous recombination of PCR products or by mating yeast strains and inducing sporulation to obtain tetrads for dissection. All yeast strains were maintained on standard yeast growth medium of either yeast extract/peptone/dextrose (YPD) medium (Fisher BP1422, BP1420, and Bioshop GLU501) or synthetic complete (SC) medium (BD 291920) with appropriate amino acid dropouts and 2% dextrose. Yeast cultures were grown at 30°C.

Plasmids and constructs

Coding sequences for plasmid construction were obtained by PCR amplification of genomic DNA extracts from BY4741 yeast. For MBP-tagged Osh6 for bacterial expression, the coding sequence of Osh6 was inserted into pMAL-C2X (NEB) using BamHI and HindIII cut sites. Similarly, Ist2 amplified sequences were inserted into pGEX-6P2 (GE) using BamHI and XmaI cut sites.

The coding sequence of Ist2 along with its native promoter and 3′ UTR sequences was cloned using the same sequences as in the MoBY-ORF collection (Ho et al., 2009) and inserted into pRS416 using XmaI and EagI restriction enzymes to yield p416-Ist2. To delete residues 732–747 in this construct, the sequence corresponding to amino acid residues 681–877 was synthesized (IDT), digested with AgeI and AflII, and inserted into similarly digested p416-Ist2 to yield p416-Ist2Δ732–747.

To construct p416-Snd3-GFP-Ist2$^{589–946}$, the coding sequence corresponding to Ist2 amino acid residues 589–946 was inserted using MfeI and SacI cut sites into p416-Snd3-GFP (also known as p416-Pho88-GFP), with expression driven by the constitutive portion of the PHO5 promoter (Chao et al., 2014). To construct p416-Ist2Δ732–747-GFP, p416-Snd3-GFP was digested with BamHI and AgeI and inserted with an Ist2Δ732–747 coding sequence amplified off p416-Ist2Δ732–747 and digested with BamHI and XmaI.

To construct p413-Osh6-DHFR[3], p413-Scs2ΔTM-DHFR[3] containing the constitutive portion of the PHO5 promoter (Chao et al., 2014) was digested with BamHI to remove the Scs2 sequence and inserted with the coding sequence of Osh6 to yield p413-Osh6-DHFR[3], containing an extra XmaI site. p413-Osh6-DHFR[3] was digested with BamHI to remove the Osh6 sequence and inserted with full-length Ist2 and Ist2Δ732–747 sequences to yield p413-Ist2-DHFR[3] and p413-Ist2Δ732–747-DHFR[3], respectively. Additionally, p413-Osh6-DHFR[3] was digested with EagI and XmaI to obtain p413-Ist2-732–747-DHFR[3], p413-Ist2-727–776-DHFR[3], and p413-Osh7-DHFR[3].

Galactose-driven overexpression plasmids were obtained from the FLEX overexpression library (Hu et al., 2007) generously provided by Megan Kofoed (Michael Smith Laboratories, University of British Columbia, Vancouver, Canada) from the laboratory of Phil Hieter. All FLEX plasmids were sequenced to confirm their identity. Osh6 and Osh7 L69D mutants were generated using the NEB Q5 Site-Directed Mutagenesis kit (E0554), with primer pairs 5′-CAGGATCACCGATCCTACTTTTATTTTAGAAAAAAAATC-3′ and 5′ GTCAAATCGCAGCCTGGT-3′ for Osh6 and 5′-TAGAATCACAGATCCGACATTTATTCTGG-3′ and 5′ GATAAATCACAACCTGGC-3′ for Osh7.

Growth assays

Yeast was grown overnight in liquid in SC medium supplemented with 1 mM Cho (or 1 mM Etn in the case of *Δdpl1* deletion mutants), diluted into fresh medium, and then grown until

reaching logarithmic growth phase (OD_{600} 0.2–0.5). Cells were then centrifuged at 2,000 *g* for 1 min and washed three times with water to remove residual Cho, before being transferred to liquid or solid medium. For DHFR PCAs, cells were grown without Cho supplementation and not washed before transfer.

For liquid growth assays, strains were normalized to the same OD_{600} and diluted to an OD_{600} value of 0.005–0.010 in 96-well plates in triplicate wells to a volume of 200 µl. Myriocin (M1177; Sigma-Aldrich) was added at the concentrations indicated in the text in 0.4% DMSO. Plates were then incubated at 30°C with orbital shaking at 600 rpm in a Biotek Instruments Epoch 2 Microplate Spectrophotometer. Data were $\log_2$ transformed, and appropriate time points were fitted to a linear equation, with exponential growth constants derived from the slopes of the linear equation. Statistical analysis was performed in GraphPad Prism 6, and significant differences between all pairwise combinations of groups were detected using one-way ANOVA with post hoc multiple comparisons correction using Tukey's method.

For spot assays on solid medium, cells were grown on SC agar plates containing dextrose, except for overexpression experiments where plates contained 2% galactose as indicated. Plasmids were maintained with appropriate dropouts. Some agar batches were found to be of low purity (with noticeable discoloration) and could partially support growth of *Δpsd2Δpsd1*, *Δist2Δpsd1*, and *Δosh6Δosh7Δpsd1* deletion mutants, likely indicating residual Etn/Cho in the agar. Thus, all growth assays were done using one agar batch (Laboratory Grade, AGR003, lot 8L9900; Bioshop). Agar can also be substituted with agarose. Plates with dextrose were incubated for 2 d at 30°C, whereas galactose plates were incubated for 3–5 d at 30°C. For DHFR PCAs, cells were grown on SC medium supplemented with 200 µg/ml methotrexate delivered in 1% DMSO, with plates containing the DMSO control incubated at 30°C for 2 d, whereas plates containing methotrexate were incubated for 3–4 d at 30°C. LatA (10-2254; Focus Biomolecules) was supplemented to 1.5 or 3 µM and delivered in 0.5% DMSO, with plates incubated for 3 d at 30°C. For both liquid growth assays and spot assays, Etn and Cho were supplemented at 1 mM where indicated.

Measurement of steady-state PE Levels

40 OD_{600} units of log-phase cells grown in SC medium without Etn or Cho were harvested by centrifugation at 3,000 *g* for 3 min. LatA treatment was performed for 24 h at 1.5 µm in 0.5% DMSO. Cell pellets were disrupted with glass beads (G8772), and the bead supernatant was extracted twice with 800 µl water; the extracts (1.6 ml total) were added directly to 36 ml of 2:1 methanol:chloroform, to which 8 ml water was then added. The mixture was vortexed, 12 ml of 0.9% NaCl solution was added, and it was vortexed again and centrifuged at 1,000 *g* for 5 min to achieve phase separation. The lower organic layer was withdrawn and evaporated under nitrogen gas and redissolved in 100 µl of chloroform. 30 µl of the lipid solution was then spotted onto silica gel TLC plates (CA1.05554.0001; VWR), and the plates were developed with 75:25:4 chloroform:methanol:water (Knittelfelder and Kohlwein, 2017). Spot identities were confirmed with lipid standards and ninhydrin staining. Densitometry was performed with ImageJ (National Institutes of Health). Statistical analysis was performed in GraphPad Prism 6, and significant differences between all pairwise combinations of groups were detected using one-way ANOVA with post hoc multiple comparisons correction using Tukey's method. Data distribution was assumed to be normal but was not formally tested.

Confocal microscopy

Log-phase live yeast cells were imaged on either an Olympus FV1000 system equipped with differential interference contrast imaging using a 60× Plan Apochromat objective (NA 1.35; oil). Images were captured using Olympus Fluoview FV10-ASW software and analyzed using the Fiji distribution (Schindelin et al., 2012) of ImageJ software (Rueden et al., 2017). To quantify nuclear-to-cortical ER localization ratios of Ist2-GFP, cells were identified that contained clearly visible nuclei as marked by the ER marker RFP-ER, a fusion protein of RFP with the transmembrane helix of Scs2 (Loewen et al., 2007). Regions of interest (ROIs) were then selected with the Selection Brush tool, and the average fluorescence intensity of Ist2-GFP at the nuclear ER and the cortical ER were divided to obtain the ratio. For Osh6/7-GFP, ROIs were selected for pmaER using RFP-ER as a marker, whereas cytosolic ROIs were picked from the interior of the cell. For experiments without RFP-ER, ROIs at the cell periphery and the cytosol were selected using differential interference contrast/bright-field images as a guide. Ratios were normalized to the mean of WT cells for each experiment. Statistical analysis was performed in GraphPad Prism 6, and significant differences between all pairwise combinations of groups were detected using one-way ANOVA with post hoc multiple comparisons correction using Tukey's method. For single comparisons, differences were detected by unpaired *t* tests. Data distribution was assumed to be normal but was not formally tested.

In vitro protein interaction assay of Ist2 peptides with Osh6

Escherichia coli harboring pMBP-Osh6 were grown in 800-ml cultures until log phase, and expression was induced with 0.5 mM IPTG (IPT001; Bioshop) overnight at 18°C. Cells were harvested, frozen at −80°C, and lysed by probe sonication in lysis buffer (50 mM Tris HCl, pH 7.4, and 120 mM NaCl) containing 1 mM 4-(2-aminoethyl)benzenesulfonyl fluoride hydrochloride (AEB602; Bioshop) and 1 mM DTT. Lysates were cleared by centrifugation at 15,000 *g* for 20 min, and the supernatant was incubated with amylose resin (NEB). The resin was washed with lysis buffer, and the bound proteins were eluted with lysis buffer containing 20 mM maltose.

Similarly, GST-Ist2 peptide fusion proteins and GST were grown to log phase in 100-ml cultures, and expression was induced with 0.25 mM IPTG for 3 h. The cells were frozen at −80°C, lysed by probe sonication in lysis buffer, bound to glutathione Sepharose 4B resin (GE), and washed with binding buffer (lysis buffer containing 0.1% Igepal CA630; I8896; Sigma-Aldrich) before further analysis.

To assess protein interaction, 50 µl of bound GST-Ist2 peptide fusion protein resin slurry was incubated with 50 µl of MBP-Osh6 in solution with 900 µl of binding buffer for 1 h at 4°C,

washed three times with binding buffer, heated at 65°C for 10 min in Laemmli sample buffer, and subjected to analysis on SDS-PAGE gels with Coomassie Blue staining. Stained gels were imaged with a flatbed scanner.

SGA analysis

Creation of the genome-wide array of double mutants with *Δpsd1* deletion strain was undertaken as previously described (Tong and Boone, 2006). Briefly, *PSD1* was knocked out in the SGA query background Y7092 using a NatMX cassette amplified off p4339. This *Δpsd1* query strain was mated with an array of nonessential deletion mutants containing kanMX markers, and the diploids were selected and induced to undergo sporulation. From spores, *MAT*a cells were obtained, separately pinned onto plates containing the drug G418 or both G418 and clonNAT, and repinned onto drug-containing medium. Results were analyzed using Balony software (Young and Loewen, 2013). Gene ontology term enrichment and protein–protein interaction network analysis were performed using the GeneMANIA webserver, with gene ontology term enrichment presented as Benjamini–Hochberg false discovery rate–adjusted P values (*q* values) from hypergeometric tests (Warde-Farley et al., 2010; Zuberi et al., 2013).

Protein alignments and disordered sequence prediction

Ist2 alignments with fungal homologues were generated from the Fungal Orthogroups Repository (Wapinski et al., 2007). Disordered protein sequence prediction was generated with DISOPRED3 (Jones and Cozzetto, 2015).

Online supplemental material

Fig. S1 shows additional micrographs and other data supporting the localization and interaction of Ist2/Osh6/Osh7 in Fig. 1. Fig. S2 shows growth curves and all growth constants from Fig. 2. Fig. S3 shows additional control growth assays supporting Fig. 3 and Fig. 4. Fig. S4 shows representative TLC plates from Fig. 8 and strong negative genetic interactors of *PSD1* that are rescued by Etn addition (SGA screen). Fig. S5 shows supporting growth curve analysis and additional control growth assays supporting Fig. 9 and representative TLC plates. Table S1 and Table S2 list the yeast strains and plasmids used in this study, respectively.

Acknowledgments

We thank Tim Levine and Elizabeth Conibear for critical discussions. We thank Phil Hieter for plasmids.

Research was funded by the Canadian Institutes of Health Research (MOP-79497) and the Natural Sciences and Engineering Research Council of Canada (RGPIN-2017-05861). A.K.O. Wong was funded by a Natural Sciences and Engineering Research Council of Canada scholarship.

The authors declare no competing financial interests.

Author contributions: A.K.O. Wong conceptualized, carried out, and analyzed the experiments. B.P. Young performed and analyzed the SGA screen. C.J.R. Loewen conceptualized and analyzed the experiments. A.K.O. Wong and C.J.R. Loewen wrote the manuscript.

Submitted: 22 October 2019
Revised: 13 April 2021
Accepted: 15 June 2021

References

Alvadia, C., N.K. Lim, V. Clerico Mosina, G.T. Oostergetel, R. Dutzler, and C. Paulino. 2019. Cryo-EM structures and functional characterization of the murine lipid scramblase TMEM16F. *eLife.* 8:e44365. https://doi.org/10.7554/eLife.44365

Ayscough, K.R., J. Stryker, N. Pokala, M. Sanders, P. Crews, and D.G. Drubin. 1997. High rates of actin filament turnover in budding yeast and roles for actin in establishment and maintenance of cell polarity revealed using the actin inhibitor latrunculin-A. *J. Cell Biol.* 137:399–416. https://doi.org/10.1083/jcb.137.2.399

Babu, M., J. Vlasblom, S. Pu, X. Guo, C. Graham, B.D.M. Bean, H.E. Burston, F.J. Vizeacoumar, J. Snider, S. Phanse, et al. 2012. Interaction landscape of membrane-protein complexes in Saccharomyces cerevisiae. *Nature.* 489:585–589. https://doi.org/10.1038/nature11354

Balderhaar, H.J., and C. Ungermann. 2013. CORVET and HOPS tethering complexes - coordinators of endosome and lysosome fusion. *J. Cell Sci.* 126:1307–1316. https://doi.org/10.1242/jcs.107805

Beh, C.T., L. Cool, J. Phillips, and J. Rine. 2001. Overlapping functions of the yeast oxysterol-binding protein homologues. *Genetics.* 157:1117–1140. https://doi.org/10.1093/genetics/157.3.1117

Besprozvannaya, M., E. Dickson, H. Li, K.S. Ginburg, D.M. Bers, J. Auwerx, and J. Nunnari. 2018. GRAM domain proteins specialize functionally distinct ER-PM contact sites in human cells. *eLife.* 7:e31019. https://doi.org/10.7554/eLife.31019

Birner, R., M. Bürgermeister, R. Schneiter, and G. Daum. 2001. Roles of phosphatidylethanolamine and of its several biosynthetic pathways in Saccharomyces cerevisiae. *Mol. Biol. Cell.* 12:997–1007. https://doi.org/10.1091/mbc.12.4.997

Bonifacino, J.S., and A. Hierro. 2011. Transport according to GARP: receiving retrograde cargo at the trans-Golgi network. *Trends Cell Biol.* 21:159–167. https://doi.org/10.1016/j.tcb.2010.11.003

Boone, C., H. Bussey, and B.J. Andrews. 2007. Exploring genetic interactions and networks with yeast. *Nat. Rev. Genet.* 8:437–449. https://doi.org/10.1038/nrg2085

Brunner, J.D., N.K. Lim, S. Schenck, A. Duerst, and R. Dutzler. 2014. X-ray structure of a calcium-activated TMEM16 lipid scramblase. *Nature.* 516:207–212. https://doi.org/10.1038/nature13984

Chao, J.T., A.K.O. Wong, S. Tavassoli, B.P. Young, A. Chruscicki, N.N. Fang, L.J. Howe, T. Mayor, L.J. Foster, and C.J.R. Loewen. 2014. Polarization of the endoplasmic reticulum by ER-septin tethering. *Cell.* 158:620–632. https://doi.org/10.1016/j.cell.2014.06.033

Chung, J., F. Torta, K. Masai, L. Lucast, H. Czapla, L.B. Tanner, P. Narayanaswamy, M.R. Wenk, F. Nakatsu, and P. De Camilli. 2015. INTRACELLULAR TRANSPORT. PI4P/phosphatidylserine countertransport at ORP5- and ORP8-mediated ER-plasma membrane contacts. *Science.* 349:428–432. https://doi.org/10.1126/science.aab1370

Costanzo, M., A. Baryshnikova, J. Bellay, Y. Kim, E.D. Spear, C.S. Sevier, H. Ding, J.L.Y. Koh, K. Toufighi, S. Mostafavi, et al. 2010. The genetic landscape of a cell. *Science.* 327:425–431. https://doi.org/10.1126/science.1180823

D'Ambrosio, J.M., V. Albanèse, N.F. Lipp, L. Fleuriot, D. Debayle, G. Drin, and A. Čopič. 2020. Osh6 requires Ist2 for localization to ER–PM contacts and efficient phosphatidylserine transport in budding yeast. *J. Cell Sci.* 133:jcs243733. https://doi.org/10.1242/jcs.243733

Dang, S., S. Feng, J. Tien, C.J. Peters, D. Bulkley, M. Lolicato, J. Zhao, K. Zuberbühler, W. Ye, L. Qi, et al. 2017. Cryo-EM structures of the TMEM16A calcium-activated chloride channel. *Nature.* 552:426–429. https://doi.org/10.1038/nature25024

Dixon, S.J., M. Costanzo, A. Baryshnikova, B. Andrews, and C. Boone. 2009. Systematic mapping of genetic interaction networks. *Annu. Rev. Genet.* 43:601–625. https://doi.org/10.1146/annurev.genet.39.073003.114751

Donnelly, S.F.H., M.J. Pocklington, D. Pallotta, and E. Orr. 1993. A proline-rich protein, verprolin, involved in cytoskeletal organization and cellular growth in the yeast Saccharomyces cerevisiae. *Mol. Microbiol.* 10:585–596. https://doi.org/10.1111/j.1365-2958.1993.tb00930.x

Duran, C., Z. Qu, A.O. Osunkoya, Y. Cui, and H.C. Hartzell. 2012. ANOs 3-7 in the anoctamin/Tmem16 Cl- channel family are intracellular proteins. *Am. J. Physiol. Cell Physiol.* 302:C482–C493. https://doi.org/10.1152/ajpcell.00140.2011

Eisenberg-Bord, M., N. Shai, M. Schuldiner, and M. Bohnert. 2016. A Tether Is a Tether Is a Tether: Tethering at Membrane Contact Sites. *Dev. Cell.* 39:395–409. https://doi.org/10.1016/j.devcel.2016.10.022

Encinar Del Dedo, J., F.Z. Idrissi, I.M. Fernandez-Golbano, P. Garcia, E. Rebollo, M.K. Krzyzanowski, H. Grötsch, and M.I. Geli. 2017. ORP-Mediated ER Contact with Endocytic Sites Facilitates Actin Polymerization. *Dev. Cell.* 43:588–602.e6. https://doi.org/10.1016/j.devcel.2017.10.031

Fairn, G.D., M. Hermansson, P. Somerharju, and S. Grinstein. 2011. Phosphatidylserine is polarized and required for proper Cdc42 localization and for development of cell polarity. *Nat. Cell Biol.* 13:1424–1430. https://doi.org/10.1038/ncb2351

Falzone, M.E., J. Rheinberger, B.-C. Lee, T. Peyear, L. Sasset, A.M. Raczkowski, E.T. Eng, A. Di Lorenzo, O.S. Andersen, C.M. Nimigean, and A. Accardi. 2019. Structural basis of Ca^{2+}-dependent activation and lipid transport by a TMEM16 scramblase. *eLife.* 8:e43229. https://doi.org/10.7554/eLife.43229

Fischer, M.A., K. Temmerman, E. Ercan, W. Nickel, and M. Seedorf. 2009. Binding of plasma membrane lipids recruits the yeast integral membrane protein Ist2 to the cortical ER. *Traffic.* 10:1084–1097. https://doi.org/10.1111/j.1600-0854.2009.00926.x

Franz, A., K. Maass, and M. Seedorf. 2007. A complex peptide-sorting signal, but no mRNA signal, is required for the Sec-independent transport of Ist2 from the yeast ER to the plasma membrane. *FEBS Lett.* 581:401–405. https://doi.org/10.1016/j.febslet.2006.12.048

Friedman, J.R., M. Kannan, A. Toulmay, C.H. Jan, J.S. Weissman, W.A. Prinz, and J. Nunnari. 2018. Lipid Homeostasis Is Maintained by Dual Targeting of the Mitochondrial PE Biosynthesis Enzyme to the ER. *Dev. Cell.* 44:261–270.e6. https://doi.org/10.1016/j.devcel.2017.11.023

Galmes, R., A. Houcine, A.R. van Vliet, P. Agostinis, C.L. Jackson, and F. Giordano. 2016. ORP5/ORP8 localize to endoplasmic reticulum-mitochondria contacts and are involved in mitochondrial function. *EMBO Rep.* 17:800–810. https://doi.org/10.15252/embr.201541108

Gatta, A.T., and T.P. Levine. 2017. Piecing Together the Patchwork of Contact Sites. *Trends Cell Biol.* 27:214–229. https://doi.org/10.1016/j.tcb.2016.08.010

Gatta, A.T., L.H. Wong, Y.Y. Sere, D.M. Calderón-Noreña, S. Cockcroft, A.K. Menon, and T.P. Levine. 2015. A new family of StART domain proteins at membrane contact sites has a role in ER–PM sterol transport. *eLife.* 4: e07253. https://doi.org/10.7554/eLife.07253

Goode, B.L., J.A. Eskin, and B. Wendland. 2015. Actin and endocytosis in budding yeast. *Genetics.* 199:315–358. https://doi.org/10.1534/genetics.112.145540

Goud, B., S. Liu, and B. Storrie. 2018. Rab proteins as major determinants of the Golgi complex structure. *Small GTPases.* 9:66–75. https://doi.org/10.1080/21541248.2017.1384087

Gulshan, K., P. Shahi, and W.S. Moye-Rowley. 2010. Compartment-specific synthesis of phosphatidylethanolamine is required for normal heavy metal resistance. *Mol. Biol. Cell.* 21:443–455. https://doi.org/10.1091/mbc.e09-06-0519

Henne, W.M., N.J. Buchkovich, and S.D. Emr. 2011. The ESCRT pathway. *Dev. Cell.* 21:77–91. https://doi.org/10.1016/j.devcel.2011.05.015

Henry, S.A., S.D. Kohlwein, and G.M. Carman. 2012. Metabolism and regulation of glycerolipids in the yeast Saccharomyces cerevisiae. *Genetics.* 190:317–349. https://doi.org/10.1534/genetics.111.130286

Ho, C.H., L. Magtanong, S.L. Barker, D. Gresham, S. Nishimura, P. Natarajan, J.L.Y. Koh, J. Porter, C.A. Gray, R.J. Andersen, et al. 2009. A molecular barcoded yeast ORF library enables mode-of-action analysis of bioactive compounds. *Nat. Biotechnol.* 27:369–377. https://doi.org/10.1038/nbt.1534

Hu, Y., A. Rolfs, B. Bhullar, T.V.S. Murthy, C. Zhu, M.F. Berger, A.A. Camargo, F. Kelley, S. McCarron, D. Jepson, et al. 2007. Approaching a complete repository of sequence-verified protein-encoding clones for Saccharomyces cerevisiae. *Genome Res.* 17:536–543. https://doi.org/10.1101/gr.6037607

Jha, A., W.Y. Chung, L. Vachel, J. Maleth, S. Lake, G. Zhang, M. Ahuja, and S. Muallem. 2019. Anoctamin 8 tethers endoplasmic reticulum and plasma membrane for assembly of Ca^{2+} signaling complexes at the ER/PM compartment. *EMBO J.* 38:e101452. https://doi.org/10.15252/embj.2018101452

Jones, D.T., and D. Cozzetto. 2015. DISOPRED3: precise disordered region predictions with annotated protein-binding activity. *Bioinformatics.* 31: 857–863. https://doi.org/10.1093/bioinformatics/btu744

Knittelfelder, O.L., and S.D. Kohlwein. 2017. Thin-Layer Chromatography to Separate Phospholipids and Neutral Lipids from Yeast. *Cold Spring Harb. Protoc.* 2017(5). https://doi.org/10.1101/pdb.prot085456

Kralt, A., M. Carretta, M. Mari, F. Reggiori, A. Steen, B. Poolman, and L.M. Veenhoff. 2015. Intrinsically disordered linker and plasma membrane-binding motif sort Ist2 and Ssy1 to junctions. *Traffic.* 16:135–147. https://doi.org/10.1111/tra.12243

Lang, A., A.T. John Peter, and B. Kornmann. 2015. ER-mitochondria contact sites in yeast: beyond the myths of ERMES. *Curr. Opin. Cell Biol.* 35:7–12. https://doi.org/10.1016/j.ceb.2015.03.002

Lees, J.A., M. Messa, E.W. Sun, H. Wheeler, F. Torta, M.R. Wenk, P. De Camilli, and K.M. Reinisch. 2017. Lipid transport by TMEM24 at ER-plasma membrane contacts regulates pulsatile insulin secretion. *Science.* 355: eaah6171. https://doi.org/10.1126/science.aah6171

Lipp, N.F., R. Gautier, M. Magdeleine, M. Renard, V. Albanèse, A. Čopič, and G. Drin. 2019. An electrostatic switching mechanism to control the lipid transfer activity of Osh6p. *Nat. Commun.* 10:3926. https://doi.org/10.1038/s41467-019-11780-y

Loewen, C.J.R., B.P. Young, S. Tavassoli, and T.P. Levine. 2007. Inheritance of cortical ER in yeast is required for normal septin organization. *J. Cell Biol.* 179:467–483. https://doi.org/10.1083/jcb.200708205

Maeda, K., K. Anand, A. Chiapparino, A. Kumar, M. Poletto, M. Kaksonen, and A.C. Gavin. 2013. Interactome map uncovers phosphatidylserine transport by oxysterol-binding proteins. *Nature.* 501:257–261. https://doi.org/10.1038/nature12430

Malvezzi, M., M. Chalat, R. Janjusevic, A. Picollo, H. Terashima, A.K. Menon, and A. Accardi. 2013. Ca2+-dependent phospholipid scrambling by a reconstituted TMEM16 ion channel. *Nat. Commun.* 4:2367. https://doi.org/10.1038/ncomms3367

Manford, A.G., C.J. Stefan, H.L. Yuan, J.A. Macgurn, and S.D. Emr. 2012. ER-to-plasma membrane tethering proteins regulate cell signaling and ER morphology. *Dev. Cell.* 23:1129–1140. https://doi.org/10.1016/j.devcel.2012.11.004

Michnick, S.W., P.H. Ear, C. Landry, M.K. Malleshaiah, and V. Messier. 2010. A Toolkit of Protein-Fragment Complementation Assays for Studying and Dissecting Large-Scale and Dynamic Protein–Protein Interactions in Living Cells. Methods Enzymol. 470:335–368.

Milenkovic, V.M., M. Brockmann, H. Stöhr, B.H. Weber, and O. Strauss. 2010. Evolution and functional divergence of the anoctamin family of membrane proteins. *BMC Evol. Biol.* 10:319. https://doi.org/10.1186/1471-2148-10-319

Miller, V.J., and D. Ungar. 2012. Re'COG'nition at the Golgi. *Traffic.* 13:891–897. https://doi.org/10.1111/j.1600-0854.2012.01338.x

Moser von Filseck, J., A. Čopič, V. Delfosse, S. Vanni, C.L. Jackson, W. Bourguet, and G. Drin. 2015. INTRACELLULAR TRANSPORT. Phosphatidylserine transport by ORP/Osh proteins is driven by phosphatidylinositol 4-phosphate. *Science.* 349:432–436. https://doi.org/10.1126/science.aab1346

Munn, A.L., B.J. Stevenson, M.I. Geli, and H. Riezman. 1995. end5, end6, and end7: mutations that cause actin delocalization and block the internalization step of endocytosis in Saccharomyces cerevisiae. *Mol. Biol. Cell.* 6:1721–1742. https://doi.org/10.1091/mbc.6.12.1721

Naqvi, S.N., R. Zahn, D.A. Mitchell, B.J. Stevenson, and A.L. Munn. 1998. The WASp homologue Las17p functions with the WIP homologue End5p/verprolin and is essential for endocytosis in yeast. *Curr. Biol.* 8:959–962. https://doi.org/10.1016/S0960-9822(98)70396-3

Pelz, T., D.R. Drose, D. Fleck, B. Henkel, T. Ackels, M. Spehr, and E.M. Neuhaus. 2018. An ancestral TMEM16 homolog from Dictyostelium discoideum forms a scramblase. *PLoS One.* 13:e0191219. https://doi.org/10.1371/journal.pone.0191219

Pichler, H., B. Gaigg, C. Hrastnik, G. Achleitner, S.D. Kohlwein, G. Zellnig, A. Perktold, and G. Daum. 2001. A subfraction of the yeast endoplasmic reticulum associates with the plasma membrane and has a high capacity to synthesize lipids. *Eur. J. Biochem.* 268:2351–2361. https://doi.org/10.1046/j.1432-1327.2001.02116.x

Pietrangelo, A., and N.D. Ridgway. 2018. Bridging the molecular and biological functions of the oxysterol-binding protein family. *Cell. Mol. Life Sci.* 75:3079–3098. https://doi.org/10.1007/s00018-018-2795-y

Quon, E., Y.Y. Sere, N. Chauhan, J. Johansen, D.P. Sullivan, J.S. Dittman, W.J. Rice, R.B. Chan, G. Di Paolo, C.T. Beh, and A.K. Menon. 2018. Endoplasmic reticulum-plasma membrane contact sites integrate sterol and phospholipid regulation. *PLoS Biol.* 16:e2003864. https://doi.org/10.1371/journal.pbio.2003864

Ramesh, N., I.M. Antón, J.H. Hartwig, and R.S. Geha. 1997. WIP, a protein associated with wiskott-aldrich syndrome protein, induces actin polymerization and redistribution in lymphoid cells. *Proc. Natl. Acad. Sci. USA.* 94:14671–14676. https://doi.org/10.1073/pnas.94.26.14671

Raychaudhuri, S., and W.A. Prinz. 2010. The diverse functions of oxysterol-binding proteins. *Annu. Rev. Cell Dev. Biol.* 26:157–177. https://doi.org/10.1146/annurev.cellbio.042308.113334

Riekhof, W.R., W.I. Wu, J.L. Jones, M. Nikrad, M.M. Chan, C.J.R. Loewen, and D.R. Voelker. 2014. An assembly of proteins and lipid domains regulates transport of phosphatidylserine to phosphatidylserine decarboxylase 2 in Saccharomyces cerevisiae. *J. Biol. Chem.* 289:5809–5819. https://doi.org/10.1074/jbc.M113.518217

Rueden, C.T., J. Schindelin, M.C. Hiner, B.E. DeZonia, A.E. Walter, E.T. Arena, and K.W. Eliceiri. 2017. ImageJ2: ImageJ for the next generation of scientific image data. *BMC Bioinformatics.* 18:529. https://doi.org/10.1186/s12859-017-1934-z

Saheki, Y., and P. De Camilli. 2017. Endoplasmic Reticulum-Plasma Membrane Contact Sites. *Annu. Rev. Biochem.* 86:659–684. https://doi.org/10.1146/annurev-biochem-061516-044932

Saheki, Y., X. Bian, C.M. Schauder, Y. Sawaki, M.A. Surma, C. Klose, F. Pincet, K.M. Reinisch, and P. De Camilli. 2016. Control of plasma membrane lipid homeostasis by the extended synaptotagmins. *Nat. Cell Biol.* 18:504–515. https://doi.org/10.1038/ncb3339

Sandhu, J., S. Li, L. Fairall, S.G. Pfisterer, J.E. Gurnett, X. Xiao, T.A. Weston, D. Vashi, A. Ferrari, J.L. Orozco, et al. 2018. Aster Proteins Facilitate Nonvesicular Plasma Membrane to ER Cholesterol Transport in Mammalian Cells. *Cell.* 175:514–529.e20. https://doi.org/10.1016/j.cell.2018.08.033

Schindelin, J., I. Arganda-Carreras, E. Frise, V. Kaynig, M. Longair, T. Pietzsch, S. Preibisch, C. Rueden, S. Saalfeld, B. Schmid, et al. 2012. Fiji: an open-source platform for biological-image analysis. *Nat. Methods.* 9:676–682. https://doi.org/10.1038/nmeth.2019

Schulz, T.A., M.G. Choi, S. Raychaudhuri, J.A. Mears, R. Ghirlando, J.E. Hinshaw, and W.A. Prinz. 2009. Lipid-regulated sterol transfer between closely apposed membranes by oxysterol-binding protein homologues. *J. Cell Biol.* 187:889–903. https://doi.org/10.1083/jcb.200905007

Sheff, M.A., and K.S. Thorn. 2004. Optimized cassettes for fluorescent protein tagging in Saccharomyces cerevisiae. *Yeast.* 21:661–670. https://doi.org/10.1002/yea.1130

Stefan, C.J., A.G. Manford, D. Baird, J. Yamada-Hanff, Y. Mao, and S.D. Emr. 2011. Osh proteins regulate phosphoinositide metabolism at ER-plasma membrane contact sites. *Cell.* 144:389–401. https://doi.org/10.1016/j.cell.2010.12.034

Storey, M.K., K.L. Clay, T. Kutateladze, R.C. Murphy, M. Overduin, and D.R. Voelker. 2001. Phosphatidylethanolamine has an essential role in Saccharomyces cerevisiae that is independent of its ability to form hexagonal phase structures. *J. Biol. Chem.* 276:48539–48548. https://doi.org/10.1074/jbc.M109043200

Sun, Y., A.C. Martin, and D.G. Drubin. 2006. Endocytic internalization in budding yeast requires coordinated actin nucleation and myosin motor activity. *Dev. Cell.* 11:33–46. https://doi.org/10.1016/j.devcel.2006.05.008

Tavassoli, S., J.T. Chao, B.P. Young, R.C. Cox, W.A. Prinz, A.I.P.M. de Kroon, and C.J.R. Loewen. 2013. Plasma membrane--endoplasmic reticulum contact sites regulate phosphatidylcholine synthesis. *EMBO Rep.* 14:434–440. https://doi.org/10.1038/embor.2013.36

Tong, A.H.Y., and C. Boone. 2006. Synthetic Genetic Array Analysis in Saccharomyces cerevisiae. *In* Yeast Protocols. W. Xiao, editor. Humana Press, Totowa, NJ. 171–191.

Trotter, P.J., and D.R. Voelker. 1995. Identification of a non-mitochondrial phosphatidylserine decarboxylase activity (PSD2) in the yeast Saccharomyces cerevisiae. *J. Biol. Chem.* 270:6062–6070. https://doi.org/10.1074/jbc.270.11.6062

Ungermann, C., and W. Wickner. 1998. Vam7p, a vacuolar SNAP-25 homolog, is required for SNARE complex integrity and vacuole docking and fusion. *EMBO J.* 17:3269–3276. https://doi.org/10.1093/emboj/17.12.3269

van Meer, G., D.R. Voelker, and G.W. Feigenson. 2008. Membrane lipids: where they are and how they behave. *Nat. Rev. Mol. Cell Biol.* 9:112–124. https://doi.org/10.1038/nrm2330

Wagner, A., F. Di Bartolomeo, I. Klein, C. Hrastnik, K.N. Doan, T. Becker, and G. Daum. 2018. Identification and characterization of the mitochondrial membrane sorting signals in phosphatidylserine decarboxylase 1 from Saccharomyces cerevisiae. *Biochim. Biophys. Acta Mol. Cell Biol. Lipids.* 1863:117–125. https://doi.org/10.1016/j.bbalip.2017.11.003

Wapinski, I., A. Pfeffer, N. Friedman, and A. Regev. 2007. Natural history and evolutionary principles of gene duplication in fungi. *Nature.* 449:54–61. https://doi.org/10.1038/nature06107

Warde-Farley, D., S.L. Donaldson, O. Comes, K. Zuberi, R. Badrawi, P. Chao, M. Franz, C. Grouios, F. Kazi, C.T. Lopes, et al. 2010. The GeneMANIA prediction server: biological network integration for gene prioritization and predicting gene function. *Nucleic Acids Res.* 38(suppl_2):W214–W220. https://doi.org/10.1093/nar/gkq537

West, M., N. Zurek, A. Hoenger, and G.K. Voeltz. 2011. A 3D analysis of yeast ER structure reveals how ER domains are organized by membrane curvature. *J. Cell Biol.* 193:333–346. https://doi.org/10.1083/jcb.201011039

Wu, H., P. Carvalho, and G.K. Voeltz. 2018. Here, there, and everywhere: The importance of ER membrane contact sites. *Science.* 361:eaan5835. https://doi.org/10.1126/science.aan5835

Young, B.P., and C.J.R. Loewen. 2013. Balony: a software package for analysis of data generated by synthetic genetic array experiments. *BMC Bioinformatics.* 14:354. https://doi.org/10.1186/1471-2105-14-354

Zewe, J.P., R.C. Wills, S. Sangappa, B.D. Goulden, and G.R.V. Hammond. 2018. SAC1 degrades its lipid substrate PtdIns4*P* in the endoplasmic reticulum to maintain a steep chemical gradient with donor membranes. *eLife.* 7:e35588. https://doi.org/10.7554/eLife.35588

Zuberi, K., M. Franz, H. Rodriguez, J. Montojo, C.T. Lopes, G.D. Bader, and Q. Morris. 2013. GeneMANIA prediction server 2013 update. *Nucleic Acids Res.* 41:W115–W122. https://doi.org/10.1093/nar/gkt533

Supplemental material

https://doi.org/10.1083/jcb.201910161

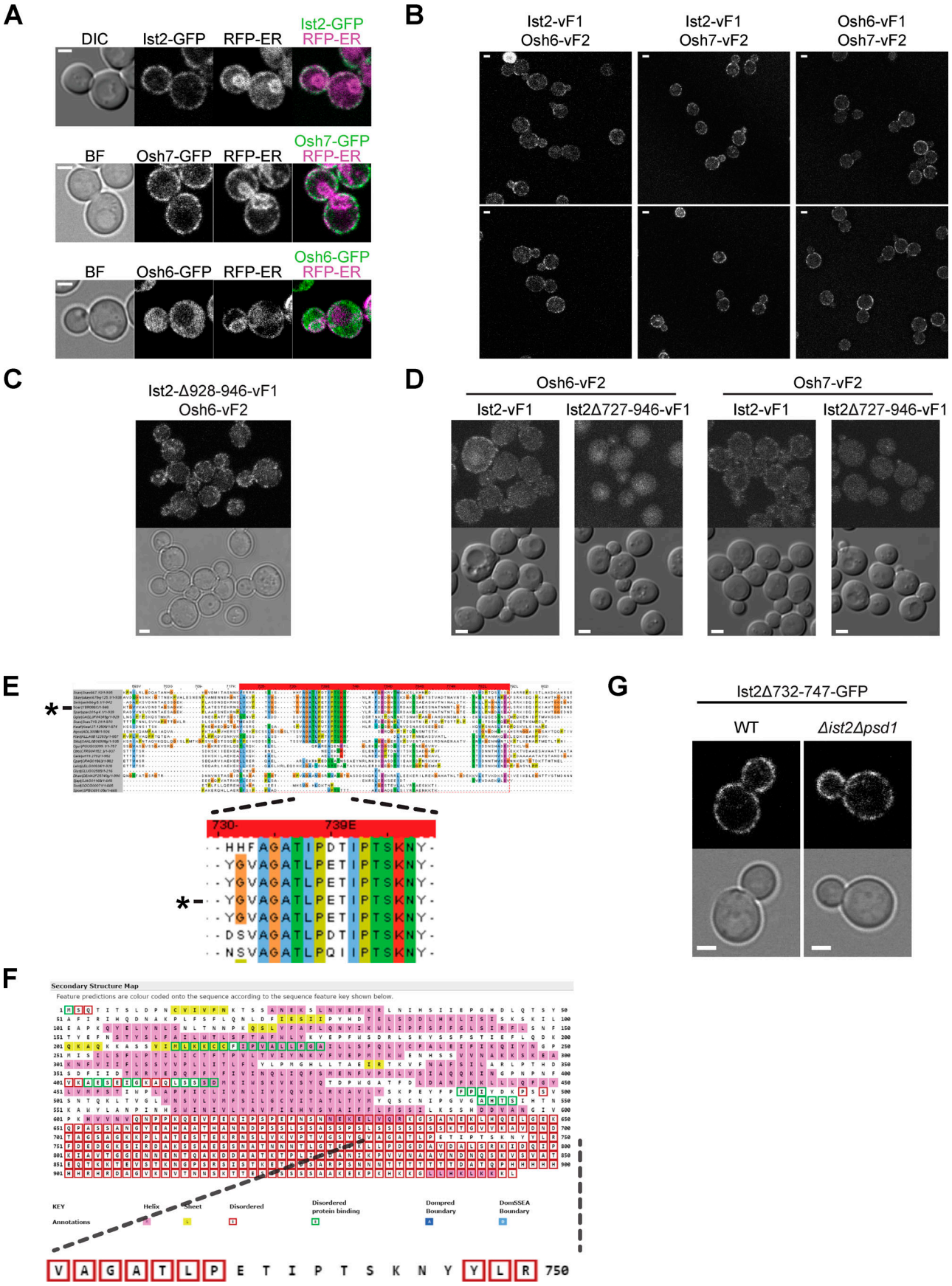
A
DIC
Ist2-GFP
RFP-ER
Ist2-GFP RFP-ER
BF
Osh7-GFP
RFP-ER
Osh7-GFP RFP-ER
BF
Osh6-GFP
RFP-ER
Osh6-GFP RFP-ER
B
Ist2-vF1 Osh6-vF2
Ist2-vF1 Osh7-vF2
Osh6-vF1 Osh7-vF2
C
Ist2-Δ928-946-vF1 Osh6-vF2
D
Osh6-vF2
Ist2-vF1
Ist2Δ727-946-vF1
Osh7-vF2
Ist2-vF1
Ist2Δ727-946-vF1
E
730-
739E
HHFAGATIPDTIPTSKNY
YGVAGATLPETIPTSKNY
YGVAGATLPETIPTSKNY
YGVAGATLPETIPTSKNY
YGVAGATLPETIPTSKNY
DSVAGATLPDTIPTSKNY
NSVAGATLPQIIPTSKNY
F
Secondary Structure Map
Feature predictions are colour coded onto the sequence according to the sequence feature key shown below.
KEY
Annotations
Helix
Sheet
Disordered
Disordered protein binding
Dompred Boundary
DomSSEA Boundary
V A G A T L P E T I P T S K N Y Y L R 750
G
Ist2Δ732-747-GFP
WT
Δist2Δpsd1

Figure S1. **Supporting data for Fig. 1. (A)** Yeast expressing genomically tagged GFP constructs and a plasmid-borne ER marker consisting of RFP fused to the C-terminal transmembrane helix of the ER protein Scs2 (RFP-ER). **(B–D)** Venus PCA with yeast expressing genomically integrated C-terminal protein fusions with Venus fragments vF1 and vF2. **(B)** Additional micrographs of cells containing Ist2, Osh6, and Osh7 PCA pairs. **(C)** Ist2 deleted for its amphipathic PM-binding helix still interacts with Osh6. **(D)** Ist2 missing most of its ER-to-PM linker no longer interacts with Osh6/7. **(E)** Alignment of the Ist2 linker region with fungal homologues. Asterisk indicates the *Saccharomyces cerevisiae* Ist2 sequence. Residue numbering is according to *S. cerevisiae* Ist2. The top panel displays the alignment of Ist2 with fungal homologue residues from residues 690 to 811. The bottom panel displays the alignment from residues 732–747. Fungal species are from the phylum Ascomycota. Species with homologues highly conserved around residues 732–747 are from the family Saccharomycetaceae, whereas less conserved homologues are from the families Saccharomycetaceae, Debaryomycetaceae, and Schizosaccharomycetaceae. **(F)** DISOPRED disordered protein sequence prediction. Red boxes indicate residues predicted to be in a disordered region. Residues 739–747 are not predicted to be disordered. **(G)** WT or *Δist2Δpsd1* cells expressing plasmid-borne Ist2Δ732–747-GFP. Medium was supplemented with Etn (1 mM) and Cho (1 mM). BF, bright field. Scale bars: 2 µm.

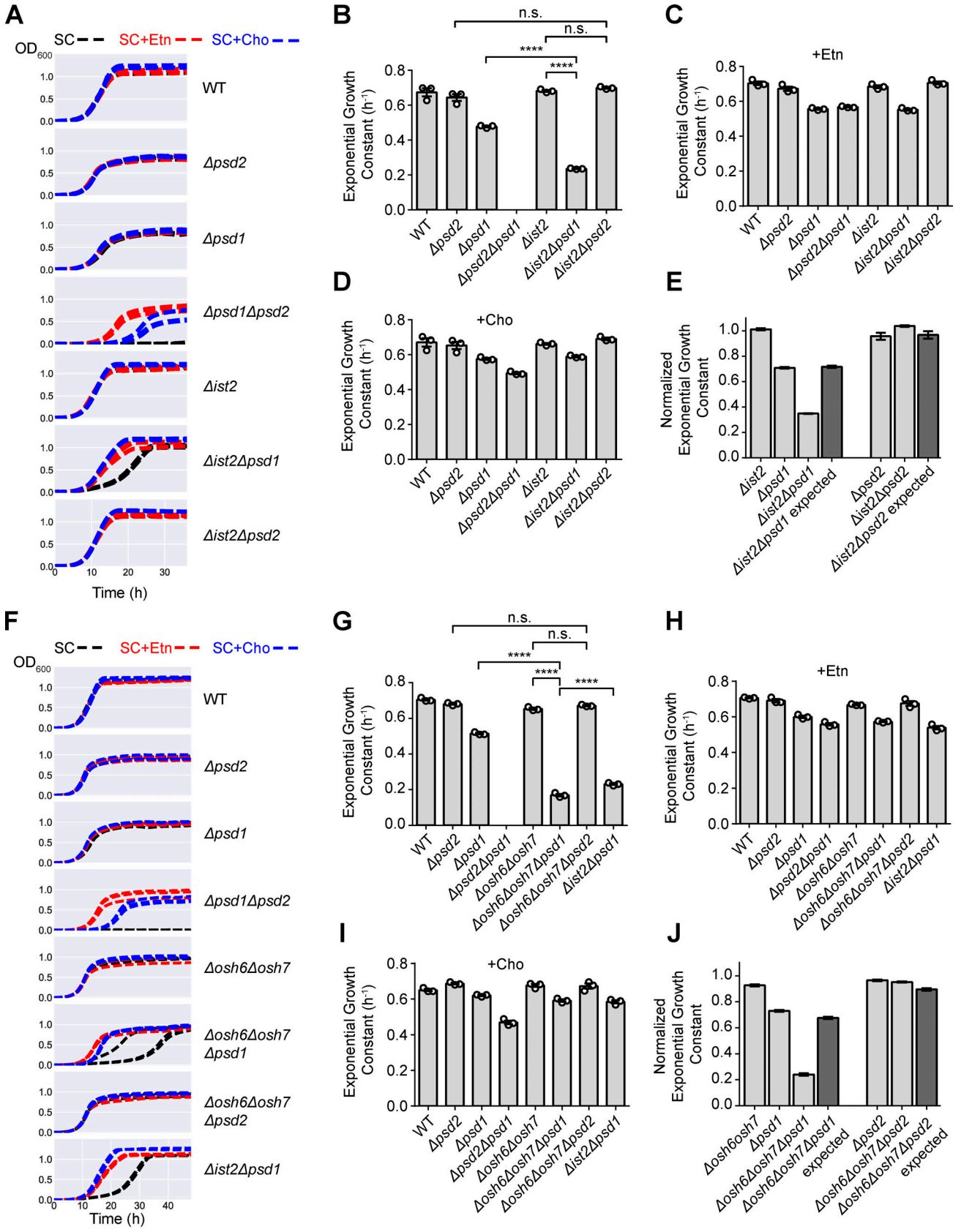

Figure S2. **Supporting data for liquid growth assays in Fig. 3. (A)** Growth curves of indicated yeast strains grown in liquid SC medium with or without Etn or Cho supplementation. **(B–D)** Base 2 exponential growth constants calculated from growth curves in A. **(E)** Exponential growth constants from B normalized to WT cells, with calculated multiplicative growth constant for *Δist2Δpsd1* and *Δist2Δpsd2* cells. **(F)** As in A. **(G–I)** As in B–D. **(J)** As in E, but with calculated multiplicative growth constant for *Δosh6Δosh7Δpsd1* and *Δosh6Δosh7Δpsd2* cells.

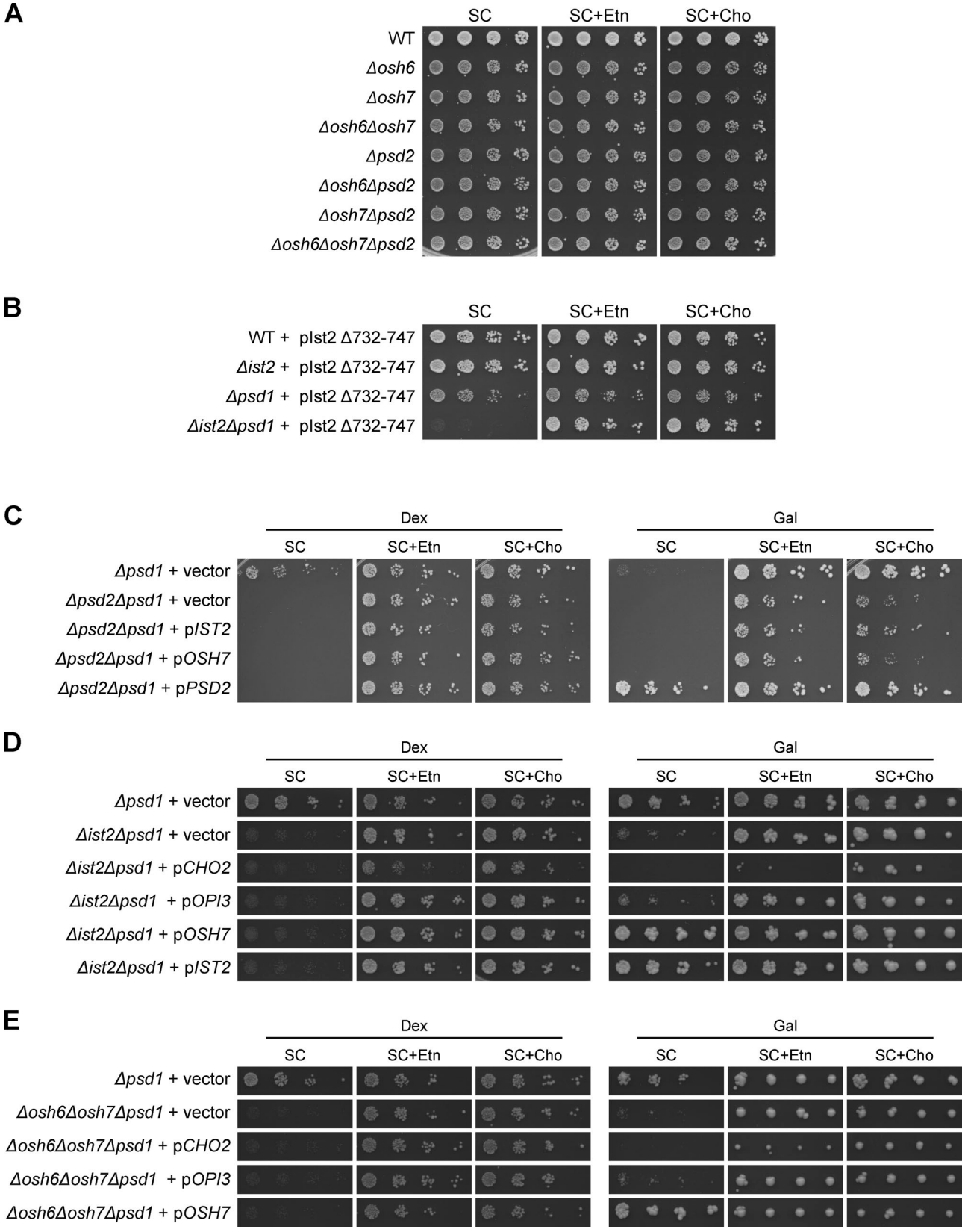

Figure S3. **Supporting data for growth assays on solid medium in Figs. 3 and 4. (A)** Serial dilutions of the indicated yeast strains grown on SC agar medium with or without Etn or Cho supplementation. **(B)** As in A, but with cells expressing plasmid-borne Ist2 mutated for its binding site with Osh6/7. **(C–E)** Serial dilutions of yeast grown on SC medium with 2% dextrose (Dex) or 2% galactose (Gal), with or without Etn or Cho supplementation, containing plasmids for overexpression of (p*OSH7*), Cho2 (p*CHO2*), Opi3 (p*OPI3*), and Ist2 (p*IST2*) under a galactose-inducible *GAL* promoter. The *GAL* promoter is repressed on dextrose. Gal-containing plates were incubated for 4 d (C) or 5 d (D and E).

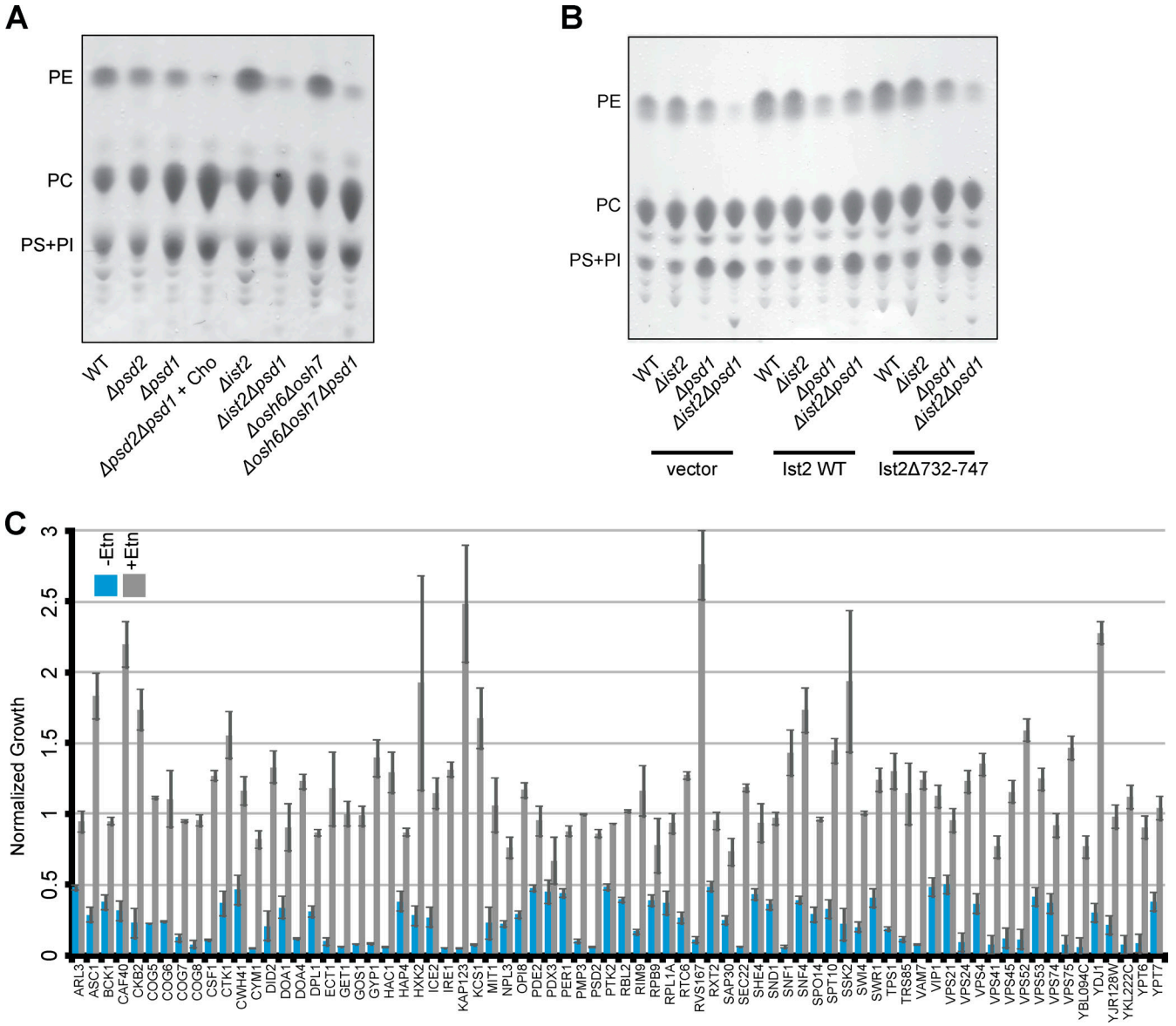

Figure S4. **Representative TLC plates and SGA screen results. (A and B)** Representative TLC plates from Fig. 8, A and B, respectively. The positions of PE, PC, and comigrating PS + PI are indicated on the left of the plate. **(C)** Normalized growth ratios for genes with strong negative genetic interactions (cutoff < 0.5) with *Δpsd1* in the absence of Etn (−Etn) and corresponding growth ratios in the presence of Etn (+Etn; related to Fig. 9). A value of 1 indicates no genetic interaction.

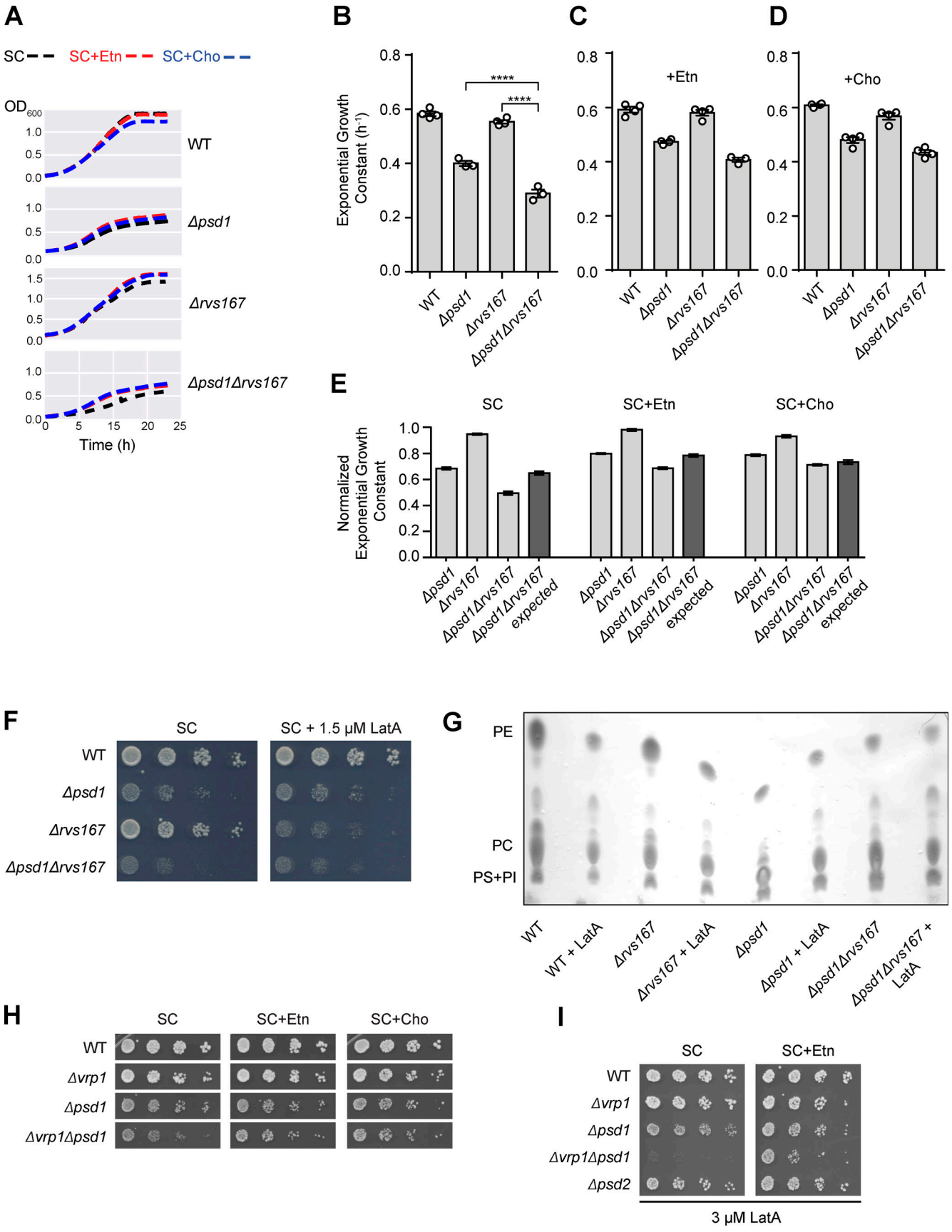

Figure S5. **Role for Endocytosis in PE synthesis. (A)** Growth curves of indicated yeast strains grown in liquid SC medium with or without Etn or Cho supplementation. **(B–D)** Base 2 exponential growth constants calculated from growth curves in A. **(E)** Exponential growth constants from B normalized to

WT cells, with calculated multiplicative growth constant for *Δpsd1Δrvs167* cells (expected). **(F)** Serial dilutions of the indicated yeast strains grown on SC agar medium with or without 1.5 µM LatA. **(G)** Representative TLC plates for lipid analysis from Fig. 9. The positions of PE, PC, and comigrating PS + PI are indicated on the left of the plate. **(H)** Serial dilutions of the indicated yeast strains grown on SC agar medium with or without Etn or Cho supplementation. **(I)** Serial dilutions of the indicated yeast strains grown on SC agar medium with or without Etn in the presence of 3 µM LatA.

Provided online are two tables. Tables S1 lists the yeast strains used in this study, respectively. Table S2 lists the plasmids used in this study, respectively.